Title

Comparative analysis of drug-salt-polymer interactions by experiment and molecular simulation improves biopharmaceutical performance

Short Title

Analysis of drug-salt-polymer interactions

Authors

Sumit Mukesh[1]†, Goutam Mukherjee[2,3]†, Ridhima Singh[1], Nathan Steenbuck[3,4], Carolina Demidova[3,5], Prachi Joshi[1], Abhay T. Sangamwar[1*], Rebecca C. Wade[2,3,6*]

Affiliations

[1] Department of Pharmaceutics, National Institute of Pharmaceutical Education and Research (NIPER), S.A.S. Nagar, Sector-67, Punjab, 160062, India.

[2] Center for Molecular Biology (ZMBH), DKFZ-ZMBH Alliance, Heidelberg University, Im Neuenheimer Feld 282, 69120 Heidelberg, Germany

[3] Molecular and Cellular Modeling Group, Heidelberg Institute forTheoretical Studies, Schloss-Wolfsbrunnenweg 35, 69118 Heidelberg, Germany

[4] Institute of Pharmacy and Molecular Biotechnology (IPMB), Heidelberg University, Im Neuenheimer Feld 364, 69120 Heidelberg, Germany

[5] Faculty of Chemistry, Heidelberg University, Im Neuenheimer Feld 364, 69120 Heidelberg, Germany

[6] Interdisciplinary Center for Scientific Computing (IWR), Heidelberg University, Im Neuenheimer Feld 205, Heidelberg, Germany

† These authors contributed equally to this work.

*Correspondence and material requests should be addressed to A.S. (email: abhays@niper.ac.in) (experiments) or to R.C.W. (email: Rebecca.wade@h-its.org) (simulations)

Abstract

The propensity of poorly water-soluble drugs to aggregate at supersaturation impedes their bioavailability. The emergence of supersaturated amorphous drug-salt-polymer systems provides a new approach to this problem. However, the effects of polymers on drug-drug interactions in aqueous phase are largely unexplored and it is unclear how to choose an optimal salt-polymer combination for a particular drug. We describe a comparative experimental and computational characterization of amorphous solid dispersions containing the drug celecoxib, and PVP-VA or HPMCAS polymers with or without Na^+/K^+ salts. Classical models for drug-polymer interactions fail to identify the best drug-salt-polymer combination. In contrast, more stable drug-polymer interaction energies computed from molecular dynamics simulations correlate with prolonged stability of supersaturated amorphous drug-salt-polymer systems, along with better dissolution and pharmacokinetic profiles. The celecoxib-salt-PVP-VA formulations exhibit excellent biopharmaceutical performance, offering the prospect of less frequent administration and lower doses of this widely used anti-inflammatory, thereby increasing cost-effectiveness, and reducing side-effects.

INTRODUCTION

Many pharmaceutical drugs are poorly water-soluble, and this property hinders their ability to reach the systemic circulation in the required concentration for optimal therapeutic effect. To overcome this problem, such drugs can be formulated in a high-energy amorphous solid state. This allows attainment of supersaturation exceeding the equilibrium solubility of the drug and thereby increases the flux across biological membranes[1-3]. However, the supersaturated state of drug molecules is metastable and therefore the drug molecules tend to aggregate and recrystallize, adversely affecting the biopharmaceutical properties of the drug[4-6]. In a typical pipeline to select excipients, such as polymers[7-9], lipids[10-12] or surfactants[13-15], to attain supersaturation of a poorly water-soluble drug (PWSD) and thereby enhance bioavailability, various supersaturated drug delivery systems are explored. A better understanding of the determinants of drug-drug and drug-excipient interactions and their relation to drug bioavailability would allow a more rational choice of drug-excipient combinations. Towards this goal, we here describe a comparative computational and experimental investigation of polymeric excipients for celecoxib (CEL) (Fig. 1A), a selective COX-2 inhibitor that is a PWSD. CEL is widely used for treating inflammatory diseases, including rheumatoid arthritis, osteoarthritis and ankylosing spondylitis,[16-18] and hence a formulation with better solubility and bioavailability would be of enormous therapeutic benefit.

The global CEL market was valued at 1149.8 million USD in 2020 and is expected to reach 1606.1 million USD by the end of 2026, growing at a CAGR (compound annual growth rate) of 8.7% from 2021 to 2026[19]. The global CEL market is mostly dominated by Pfizer, which markets CELEBREX®. CELEBREX® contains micronized CEL particles, sodium croscarmellose as a disintegrant, and povidone K30 and sodium lauryl sulphate (SLS) as solubilizers, for enhancing the solubility and oral bioavailability of CEL[20]. However, SLS is an anionic surfactant that causes strong mucosal irritation and structural modification to proteins and phospholipids, leading to toxicity in humans[21-23]. Moreover, the positive food effect observed for CELEBREX® results in varying levels of absorption of CEL. Intake of CELEBREX® is recommended with food to improve absorption, but due to differences in food intake and diet, interpatient variability in the pharmacokinetic parameters can impede correct dosing[24]. Furthermore, treatment requires the administration of high doses of CEL, generally 200-400 mg twice daily for a prolonged period for treating serious conditions, which can lead to adverse events, such as hypersensitivity reactions (anaphylaxis), abdominal pain, nasopharyngitis and arthralgia, that hamper therapy[25,26]. Thus, there is an unmet need for the development of improved dosage formulations for CEL.

We previously found that supersaturated amorphous drug-salt-polymer systems, termed amorphous salt solid dispersions (ASSD), are better than conventional binary amorphous solid dispersions (ASD) in enhancing the aqueous solubility, physical stability and bioavailability of CEL[27]. Specifically, ASSDs generated using *in situ* salt formation of CEL, which has a pK_a of 11.1, with Na^+ and K^+ counterions in the matrix of a Soluplus polymer exhibited the combined effects of solubility enhancement, stabilisation through ionic interactions between drug and counterions, and intermolecular interactions between drug and polymer, that maintain the supersaturation for prolonged times in the gastrointestinal tract (GIT)[27]. Such prolonged effects offer the prospect of lowering the dose and for once-a-day administration that together would enhance patient compliance

and reduce toxicity. Additionally, *in situ* salt formation is beneficial for pharmaceutical salts that are unstable and have tendency to undergo salt disproportionation under variable physiological and storage conditions. These findings encouraged us to investigate in the present study whether other polymers, specifically polyvinylpyrrolidone vinyl acetate (PVP-VA) and hydroxypropyl methylcellulose acetate succinate (HPMCAS) (Fig. 1B, C), might have improved effects when used with Na^+ and K^+ salts of CEL in ASSDs.

It is known that intermolecular drug-polymer interactions can significantly impact the biopharmaceutical performance[8,9,28] and physical stability[29,30] of a drug. Indeed, the general rationale for experimental screening of polymers to identify excipients for a particular drug is to identify thermodynamically miscible systems that possess adhesive interactions (specific hydrogen bonding, hydrophobic or van der Waals interactions), between the drug and the polymer in order to hinder drug-drug aggregation[31,32], and thereby prevent nucleation and crystal growth in the supersaturated solution during dissolution. The traditional methods to predict drug-polymer miscibility involve the calculation of solubility parameters and Flory-Huggins (F-H) interaction parameters[33-35]. We first applied these methods to compute solubility parameters to assess CEL-polymer miscibility for HPMCAS and PVP-VA. However, the results obtained did not correlate well with the measured physicochemical and biopharmaceutical attributes of the amorphous formulations. Therefore, we employed molecular dynamics (MD) simulations to evaluate drug-polymer interactions.

Recent studies have employed a combination of molecular docking and MD simulations[36] or MD simulations alone[37-39] to investigate interactions between drugs and excipients. Moreover, in addition to atomistic MD simulations, coarse-grained MD simulations[40,41] have been carried out to understand the mechanisms of inhibition of drug-drug aggregation in the presence of an excipient. Recently, Ouyang and colleagues developed machine learning methods to aid the selection of stable drug-polymer complexes for solid dispersion formulations and their evaluation by enthalpy calculations[42,43]. However, none of these studies estimated the strength of drug-drug interactions in the presence and absence of polymer, or in the presence of ions. Although molecular level mechanistic studies to elucidate the drug-polymer interplay in both solution and solid state have been performed using high-end analytical techniques[6,28,32], the intermolecular interactions in an aqueous environment that correlate with the *in vivo* fate of a drug remain largely unexplored, but are particularly amenable to investigation by MD simulation.

Here, MD simulations of neutral and anionic forms of CEL with different polymers, in aqueous solution, representing the *in vivo* environment, were performed, and compared with experimental measurements for novel supersaturated ASSDs that have the potential to address the aforementioned problems of drug-drug aggregation and crystallization. We find that hindrance of drug aggregation is attributable to stronger drug-polymer interactions in the ionized drug state in ASSDs compared to the non-ionized drug in conventional ASDs. Of the systems studied, the simulations reveal the most stable intermolecular interactions between anionic CEL and PVP-VA, correlating with experimental observations which show prolonged physical stability along with ameliorated solubility, dissolution, and pharmacokinetic profiles. The PVP-VA ASSD formulations enhance permeability through supersaturation-induced increased flux and thereby augment bioavailability. They thus offer the prospect of less frequent administration and lower doses with cost-effectiveness and fewer side effects, which is

particularly beneficial for the wide range of drugs that show adverse events on prolonged use.

RESULTS

Calculation of drug-polymer miscibility parameters

The Hildebrand solubility parameter (δ) of CEL and the two polymers, PVP-VA and HPMCAS, was calculated using the Fedors and Hoftyzer-Van Krevelen (HVK) group contribution methods. The difference in the δ values of CEL and each polymer was small (<7 $MPa^{1/2}$), indicating the possibility of miscibility of CEL in these polymers (Table 1). The difference was smaller for the CEL-HPMCAS system than for the CEL-PVP-VA system (0.65 vs 1.01 $MPa^{1/2}$), indicating that the CEL-HPMCAS system should have a higher miscibility than the CEL-PVP-VA system. Estimation of the Flory–Huggins (F-H) interaction parameter, χ, for the two CEL-polymer systems at 25ºC using the solubility parameter approach gave low positive values (Table 1). The closeness of the χ value for the CEL-HPMCAS system to zero suggests higher miscibility compared to the CEL-PVP-VA system at room temperature.

Preparation and characterization of formulations

Binary ASD formulations of CEL with PVP-VA or HPMCAS and ASSD formulations of CEL with Na^+ or K^+ and one of these two polymers were prepared using the components and procedure given in the Methods section and illustrated in Fig. S1. All the prepared formulations were white, free-flowing powdered solid dispersions. Optical light microscopy revealed long needle and plate-shaped crystals of CEL in non-polarised mode, and showed double refraction or birefringence in polarized mode (Fig. S2A), consistent with the anisotropic crystalline nature of many drugs[44]. All the ASD and ASSD formulations presented small spherical particles in non-polarised mode and no birefringence in polarized mode (Fig. S2(B-I)) due to isotropy and the absence of a periodic crystalline lattice, revealing their amorphous nature and indicating the role of the polymers in transforming crystalline CEL to amorphous form.

These results were further supported by Differential Scanning Calorimetry (DSC) and Powder X-ray Diffraction (PXRD). In DSC, a sharp melting endotherm was observed at 163.6°C for crystalline CEL (Fig. S3a), whereas the polymer systems lacked a sharp melting endotherm and instead exhibited broad endotherms, indicating absorbed moisture. Moreover, the observation of glass transition temperature, T_g, values in the thermograms confirmed the transformation of crystalline CEL into amorphous form in the formulations (Fig. S3b-g). These T_g values range from 71.5 to 108.8 °C and are higher than the T_g of pure amorphous CEL (59.8 °C), indicating better stability of the formulations[27]. The T_g values of the ASSDs are higher than those for the ASDs, with the highest value being observed for the CEL-K-PVP-VA ASSD. The higher T_g values for ASSD formulations with PVP-VA indicate a higher heat capacity and more rigid amorphous regions, which could be due to increased ionic interactions between the drug, counterions and polymer. In PXRD, CEL showed the characteristic peak pattern of crystalline polymorphic form III whereas a halo pattern was observed for the ASDs and ASSDs, confirming their amorphous nature (Fig. S4).

Determination of intermolecular interactions

Fourier transform infrared spectroscopy (FTIR), micro-Raman spectroscopy and nuclear magnetic resonance (NMR) spectroscopy were performed to examine the molecular interactions between CEL, in both neutral and ionic states, and the polymers in supersaturated formulations.

FTIR spectroscopy. The overlay of FTIR spectra revealed that in the amorphous formulations, the medium intensity doublet bands, corresponding to the N–H stretching of the $–NH_2$ group, were diffused and broadened, and that the asymmetric stretching vibration of the $–SO_2$ group of CEL shifted to a lower frequency in the CEL-PVP-VA ASD and disappeared in both the CEL-PVP-VA ASSDs (Fig. 2A). This indicates the participation of the $–NH_2$ group of CEL in intermolecular hydrogen bonding with the polymer[45] and the $–SO_2$ group of CEL in salt formation with the counterion due to the greater electronegativity of the oxygen atom than the nitrogen atom, which is attributed to the -R effect (negative resonance) shown by the sulphonamide group (Fig. 1A). The interaction of CEL with the counterion can also be observed in the crystal structure of the CEL-Na^+ salt[46]. The weaker electrostatic interaction between CEL and the K^+ counterion is due to the larger ionic radius and lower charge density of K^+ as compared to the Na^+ counterion[27,47].

The –C=O stretching frequency of the VA moiety of PVP-VA at 1667 cm^{-1} shifted downfield in the ASD and ASSDs, suggesting the formation of a hydrogen bond between the –C=O group of the polymer and the –NH group of CEL. The –C=O stretching frequency of the VP moiety of PVP-VA at 1731 cm^{-1} shifted in the ASSDs but there was no change in frequency for the ASD. Moreover, the –C–F symmetric stretching vibrations peak at 1228 cm^{-1} in CEL shifted to higher frequencies in all the PVP-VA and HPMCAS formulations and its intensity reduced, confirming the formation of disordered amorphous structures[48] (Fig. 2A,B).

For the CEL-HPMCAS systems, the doublet of $–NH_2$ protons of CEL at 3337 cm^{-1} and 3232 cm^{-1} shifted and broadened in all the formulations, indicating the formation of a hydrogen bond. The –S=O peak at 1346 cm^{-1} in CEL shifted to 1345 cm^{-1} in the ASD, but dissipated in both CEL-HPMCAS ASSDs, indicating salt formation. The –C=O stretching frequency of HPMCAS at 1739 cm^{-1} shifted to 1738 cm^{-1} in the ASD and 1734 cm^{-1} in the CEL-Na-HPMCAS ASSD, but disappeared in the CEL-K-HPMCAS ASSD, suggesting hydrogen bond formation between the –C=O group of the polymer and the –NH group of CEL (Fig. 2B).

These results indicate that the counterion ($Na^{+/}K^+$) interacts with CEL via strong ionic interactions resulting in salt formation. Also, the *in situ* generated salt and variations in the peak shifts suggest that CEL is hydrogen-bonded to both the –C=O groups of the PVP-VA polymer. These hydrogen bonds may help to maintain the supersaturation of CEL in solution for long times by inhibition of nucleation and crystal growth.

Micro-Raman spectroscopy. We previously described the characteristic peaks of CEL present in the micro-Raman spectrum range of 1000-1700 cm^{-1}[27] and here we focused on the same range (Fig. 2C). Crystalline CEL exhibited a characteristic peak of –S=O asymmetric stretching at 1158 cm^{-1}. The disappearance of this peak in all the CEL ASSDs confirms electrostatic interactions between the CEL –S=O group and the counterions

(Na^+/K^+), resulting in salt formation. However, the -S=O peak also disappeared in the CEL-HPMCAS ASD, which cannot be due to salt formation but may be due to its hydrogen bonding interaction with the -OH group of HPMCAS. Furthermore, the –NH peak present for crystalline CEL at 1573 cm^{-1} disappeared in all the formulations, confirming the hydrogen bonding interactions between the –NH group of CEL and the –C=O of the polymer as observed in FTIR spectra. Thus, the FTIR and micro-Raman spectroscopy both reveal *in situ* salt formation of CEL with the counterion and CEL hydrogen bonding with the polymer.

NMR spectroscopy. Chemical shifts in the aliphatic and aromatic regions of CEL as a result of alterations in the proton microenvironments were measured by NMR[32] for CEL and its amorphous formulations (Fig. S5, Fig 2D). The upfield shift in the two doublet peaks of aromatic protons attached to the sulphonamide group of CEL and the disappearance of the $–NH_2$ peak at a chemical shift of 7.52 ppm in ASSDs but not ASDs (Fig. 2D) confirmed salt formation between CEL and the counterion (Na^+/K^+) due to loss of a proton from the $–SO_2NH_2$ group, leading to shielding of the neighbouring aromatic protons in CEL. In the $–SO_2NH_2$ group, the $−NH_2$ and $−SO_2$ act as proton donor and acceptor, respectively. The $−SO_2$, being a strong electron-withdrawing group, will undergo a -R effect due to conjugation between the lone pairs of electrons of the oxygen atoms and the pi electron of the resonating system. There is a delocalisation of pi electrons towards the oxygen atoms, which further extracts electrons from the N atom of the $–NH_2$ group and leads to formation of the -S=NH bond. This effect will lead to more electron-rich oxygen atoms that can make an ionic interaction with the positively charged counterion (Fig. 1A). Furthermore, the upfield shifts of the aromatic protons in the ASSDs indicate a change in their electron density because of drug-polymer interactions. The doublet peaks of the aromatic protons in CEL at chemical shift values of 7.87 and 7.54 ppm were shifted upfield in the ASSDs, whereas no such alteration in the peaks was observed for the ASD formulations (Fig. 2D). Hydrophilic polymers can interact with drug molecules either by forming electrostatic interactions or by hydrogen bonding, thereby inhibiting drug-drug aggregation and maintaining supersaturation for prolonged times[27]. The CEL chemical shifts, along with the enhanced T_g obtained in the DSC studies, further confirm the *in situ* salt formation between CEL and the counterion (Na^+/K^+) and the drug-polymer interactions in the ASSD formulations.

Supersaturation and precipitation studies

The extent of CEL supersaturation in the ASSDs and ASDs was studied at 37 °C using an ultraviolet (UV) spectrophotometer. Excess CEL was dissolved in methanol at 5 mg/mL concentration and poured into 25 mL water. Initially, a high absorbance was observed for CEL followed by a rapid decline due to precipitation of CEL in water. The CEL-K-PVP-VA ASSD generated maximum supersaturation of CEL for 4 h due to the hydrophilic nature of the PVP-VA polymer, however the CEL-Na-PVP-VA ASSD showed a slower decline in CEL concentration for 40 min and maintained it for 4 h (Fig. S6B). This confirmed the greater hindrance of water-induced crystallization of CEL in the CEL-K-PVP-VA ASSD than in the CEL-Na-PVP-VA ASSD. CEL in the binary ASDs with both the polymers showed reduced absorbance compared to the ASSDs due to crystallization from its supersaturated state, which can be attributed to weaker intermolecular interactions between CEL and the polymer in the neutral state than in the ionic state. The ASSDs with HPMCAS were less performant in the maintenance of CEL supersaturation (Fig. S6A) due to the lower aqueous solubility of HPMCAS. The presence of the comparatively less

hydrophilic methoxy and acetate substituents makes HPMCAS water-insoluble when unionized at pH < 5 and it remains predominantly in a colloidal state at intestinal pH (i.e., pH 6.0–7.5). This ultimately results in poor aqueous solubility of the polymer even in its ionized state at the small intestinal pH and leads to the formation of colloidal polymer aggregates in aqueous solutions that promote interactions within the polymer[49]. The better behaviour of the systems containing PVP-VA than those containing HPMCAS is contrary to the predictions from the calculation of drug-polymer miscibility parameters (Table 1). Therefore, to investigate the physical mechanisms underlying the supersaturation of CEL, we next performed molecular modelling and simulation.

In silico molecular modelling

The systems simulated, labelled a-j, are listed in Table 2.

Simulation of polymers. Explicit solvent MD simulations of the individual polymers were initiated with either a PVP-VA or a HPMCAS oligomer in a rather extended modelled conformation in a periodic box of aqueous solution (Fig. 3). The oligomers of the two polymers deviated from linearity and adopted bent structures during the simulations. The all-atom root-mean-square deviation (RMSD) values showed convergence during the simulations (Fig. S7 a and b).

Simulation of CEL aggregation. Simulations were conducted to model the amorphous forms of CEL (both neutral and anionic forms) in the absence of polymer and the presence of ~0.01M NaCl (see Table 2 and Methods). CEL aggregates during simulations in aqueous solution at supersaturated concentration. The neutral form of CEL aggregated within a few hundred ns (Fig. 3). On the other hand, the anionic form of CEL only partially aggregated during one simulation (system e, final snapshot at 916 ns shown in Fig. 3) and remained dissociated during the other simulation (system f simulated for 1042 ns). In the aggregates of CEL, no specific non-covalent interactions were found, except that for neutral celecoxib, an intermolecular hydrogen bonding interaction was observed between the sulfonamide $-NH_2$ group of one CEL molecule and the $-SO_2$ group of another molecule (see radial distribution function (RDF) in Fig. 4A (a)). The same interaction was much reduced for the anionic form of CEL (Fig. 4A (b)). These results support the faster aggregation of CEL in the neutral state than in the ionic state, in the absence of polymer, due to stronger interactions between the CEL molecules.

Simulation of CEL-polymer systems. Simulations were next performed for CEL in the presence of polymer and ~0.01M NaCl and the aggregation propensities of the CEL:polymer systems was compared with the CEL-CEL systems (see Table 2 and Methods). The CEL-polymer interactions modulate the CEL:CEL hydrogen-bonding interactions. We performed two sets of MD simulations per CEL-polymer combination and analysed the trajectories in terms of hydrogen bond contact occupancy and RDFs, and computed interaction free energies with the MM/GBSA method.

Interactions between PVP-VA and CEL. For PVP-VA, a hydrogen bond (average occupancy among two sets ~43%) was observed between the sulfonamide $-NH_2$ group of CEL and the carbonyl (−C=O) group on the VP and VA moieties of PVP-VA. The RDF between the $-NH_2$ group of the neutral form of CEL and all oxygen atoms of the PVP-VA polymer shows a peak (Fig. 4B (a-b)) at 2.8±0.01 Å, whereas this peak is absent for the anionic form of CEL. In the presence of PVP-VA, the relative g(r) value in the RDF of the

CEL sulfonamide $-NH_2$ and $-SO_2$ groups is lower (Fig. 4A (c)) than in the absence of polymer (Fig. 4A (a)). Thus, the CEL:CEL hydrogen-bonding interactions are weakened by the presence of the PVP-VA oligomer.

Interactions between HPMCAS and CEL. The RDF was computed for each of the five individual functional groups of HPMCAS and for all the five groups together. The g(r) values between the neutral form of CEL and the hydroxypropoxy and hydroxyl groups of HPMCAS are the highest in both sets of simulations (Fig. 4B (e-f)). The g(r) at a distance ≤3 Å between the hydroxypropoxy group of HPMCAS and the anionic form CEL (Fig. 4B (g-h)) is less than for the neutral form of CEL, but much higher than the carbonyl oxygen of the VA group of PVP-VA (Fig. 4B (c-d)). As observed for PVP-VA, the relative g(r) value of sulfonamide−NH2 and −SO2 groups of CEL in the presence of HPMCAS, is decreased (Fig. 4A (e)) compared to in the absence of polymer (Fig. 4A (a)). Thus the CEL:CEL hydrogen-bonding interactions are also weakened by the presence of the HPMCAS oligomer.

Effect of polymers on CEL aggregation. Upon analysing the MD trajectories, we found stable CEL:oligomer complexes and a reduction in CEL:CEL interaction energy in the presence of an oligomer for the neutral form of CEL (Fig. 5 and Table S1). For the anionic form of CEL, partial or no aggregation was observed in the absence of oligomer, whereas relatively stable CEL aggregates were observed in the presence of oligomers. Of the two polymers considered here, PVP-VA formed a more stable complex with the neutral and anionic forms of CEL. Interestingly, the PVP-VA oligomer formed a relatively more stable complex with the anionic than the neutral form of CEL. This is due to the higher degree of intermolecular contact between the fluorine atoms of anionic CEL and the carbonyl carbon atoms of the PVP-VA oligomer as observed in the RDFs between these atoms (Fig. S8). This interaction strengthened the electrostatic and van der Waals forces between the PVP-VA oligomer and the anionic form of CEL (Table S2). On the other hand, the electrostatic interaction energy between the anionic form of CEL and the HPMCAS oligomer is unfavorable due to repulsive interactions between the negatively charged sulfonamide group of CEL and the oxygen atoms of the oligomer. Nevertheless, the overall energy of the complex is negative due to the favorable van der Waals and solvation energies.

We found that as the strength of oligomer:CEL interaction energy increased, the CEL:CEL interaction energy tended to decrease. The strength of the oligomer:CEL interaction is several-fold higher per CEL molecule than that of the CEL:CEL interaction in the CEL aggregate for both neutral and anionic forms of CEL. In energy component analysis, in the neutral form of the CEL aggregate, the intermolecular van der Waals component is more favourable than the electrostatic energy. For the anionic form of CEL in the presence of HPMCAS, the electrostatic energy term is highly unfavourable. However, due to the favourable solvation and van der Waals interaction energies, the overall binding free energy is favourable between CEL molecules in the anionic form and the HPMCAS oligomer. Since the CEL:PVP-VA interactions are stronger than the CEL:HPMCAS interactions for both neutral and anionic forms of CEL, PVP-VA could serve as a candidate polymer for CEL for preventing its precipitation and maintenance of supersaturation for prolonged times due to more favourable intermolecular interactions between the drug and the polymer. Notably, the order of the MM/GBSA CEL:CEL binding free energy both in neutral and anionic forms of CEL in the absence and presence of polymer, is different from that derived from the computed solubility parameters (Table

1) but correlated with the experimentally observed intermolecular interactions and biopharmaceutical performance as measured in the next section.

Solubility, dissolution and biopharmaceutical performance of the amorphous formulations

Apparent solubility studies. Apparent solubility studies performed in distilled water for 6 h showed different solubilities of CEL in its different formulations (Fig. 6A). Crystalline CEL attained the maximum solubility of 4.53 µg/mL after 30 minutes, whereas for the CEL-PVPVA and CEL-HPMCAS ASD formulations, the highest solubility obtained was 34.96 and 20.26 µg/mL, respectively after 5 minutes. For the CEL-Na-PVP-VA and CEL-K-PVP-VA ASSD formulations, the maximum solubility was attained within 5 minutes and was 736.87 and 392.48 µg/mL, respectively, whereas for the CEL-Na-HPMCAS and CEL-K-HPMCAS ASSD formulations, the maximum solubility was 73.88 and 193.19 µg/mL after 15 and 30 minutes, respectively. However, the drug concentration declined afterwards for the ASSDs, whereas no such changes were observed for the ASDs. The supersaturation was maintained for the ASSDs and the concentrations achieved after 6 hours were 139.54 and 154.72 µg/mL for CEL-Na-PVP-VA and CEL-K-PVP-VA ASSDs, respectively, and 25.54 and 126.80 µg/mL for CEL-Na-HPMCAS and CEL-K-HPMCAS ASSDs, respectively. The enhancement in solubility with respect to crystalline CEL was over 40-fold in the PVP-VA ASSDs and up to 36-fold in the CEL-K-HPMCAS ASSD. The CEL embedded in the formulations is in amorphous form, as supported by DSC and XRD spectra (see Fig. S3 and S4, respectively), and dissolved immediately in the aqueous environment (spring effect) and attained supersaturation (parachute effect). The combined effect of the loss of the crystal lattice energy and the pH buffering effect of the salt in ASSD formulations accounted for the higher apparent solubility of CEL, and extended supersaturation (see Fig. S6) due to stable intermolecular interactions. This spring and parachute phenomenon is important for significant dissolution and augmented the *in vivo* bioavailability of the drug[8].

In vitro dissolution studies. *In vitro* dissolution studies were performed to understand the release behaviour of pure crystalline CEL and CEL from amorphous ASD and ASSD formulations under sink and non-sink conditions.

Dissolution under sink conditions. The dissolution studies were performed at pH 12 using tribasic sodium phosphate buffer (1000 mL media) as recommended by the Office of Generic Drugs (OGD), USFDA. As per United State Pharmacopoeia (USP), the sink condition is defined as the condition in which one entire dose of the drug is solubilized in one third of the volume of the dissolution medium. The equilibrium solubility of pure crystalline CEL in pH 12 dissolution medium was found to be around 569.80 µg/mL. Accordingly, the entire 100 mg dose of the CEL should solubilize in 175 mL dissolution volume.

Crystalline CEL showed release of 18.73 % after 120 min whereas the formulated binary CEL-PVP-VA and CEL-HPMCAS ASDs exhibited CEL release of 88.00 % and 82.17%, respectively, after 120 min. For the CEL-Na-PVP-VA ASSD, 100.00 % of CEL was released within the initial 10 min. However, the released CEL concentration declined to 97.55 % due to its de-supersaturation after 120 min. The CEL-K-PVP-VA ASSD manifested a CEL release of 98.46 %. In the CEL-Na-HPMCAS ASSD, a rapid increase in CEL release was observed in the initial 5 min followed by supersaturation maintenance

421 over 120 min with a CEL release of 89.27 %. In contrast, the CEL-K-HPMCAS ASSD
422 showed a gradual increase in CEL release, reaching 95.67 % after 120 min, slightly higher
423 than for the CEL-Na-HPMCAS ASSD (Fig. 6B).

424 The ASD and ASSD formulations followed the concept of spring and parachute effects.
425 CEL was released rapidly above the saturation level due to its amorphous nature in the
426 formulations (spring effect), and the supersaturation was further maintained because of the
427 presence of polymer in close proximity to the drug, avoiding solution-induced
428 crystallization through drug-polymer interactions (parachute effect). For the ASSD
429 formulations, CEL solubility was enhanced due to salt formation, and the dissolution
430 performance was better than for the corresponding binary ASD, thereby achieving
431 improved bioavailability. The increment in dissolution rate is attributable to the dual
432 benefit of ASSDs, amorphization and salt formation, due to the loss of crystal lattice
433 energy and self-buffering capacity, respectively. The dissolution rate is dependent on the
434 release of drug from the diffusional double layer around the dissolving particle in the
435 medium. The salt alters the pH of the microenvironment around the dissolving drug
436 particle and promotes its ionization and faster dissolution as compared to free acid or
437 base[50].

438 *Dissolution under non-sink conditions.* Dissolution studies were performed in pH 11
439 tribasic sodium phosphate buffer. The equilibrium solubility of CEL in this buffer was
440 found to be 28.09 μg/mL. Therefore, the entire 100 mg dose of the CEL cannot be
441 solubilized in one third of the volume of the dissolution medium and the system
442 corresponds to non-sink conditions and provides a more realistic estimate of the ability of
443 amorphous solid based formulations to increase the release of PWSD in the GIT.
444 Crystalline CEL showed a low release rate of 6.96 % in pH 11 buffer after 120 min
445 because of its low solubility and poor wetting behavior. Because of its hydrophobic
446 nature, CEL tended to float on the surface of the dissolution medium during the study
447 period. The CEL release exhibited by the CEL-PVP-VA ASD was approximately 70.62 %
448 after 120 mins, which was considerably lower than for the PVP-VA ASD. On the other
449 hand, the CEL release from the CEL-HPMCAS binary ASD was higher at 81.32 %
450 compared to that for the CEL-Na-HPMCAS and CEL-K-HPMCAS ASSDs for which the
451 CEL release was 78.53 % and 68.08 %, respectively after 120 minutes (Fig. 6B),
452 indicating slow and incomplete release from the HPMCAS polymeric matrix. However,
453 both the CEL ASSD formulations displayed approximately 12-fold enhancement in the
454 percentage of drug release compared to pure crystalline CEL.

455 CEL-Na-PVP-VA and CEL-K-PVP-VA ASSD formulations exhibited a similar pattern of
456 maximum drug release, with 85.09 % and 85.98 % release after 120 mins (Fig. 6B).
457 Moreover, a difference of approximately 40 % was observed in the release profiles of
458 CEL-PVP-VA ASD and its ASSD for the initial 10 min, with the difference falling to 15
459 % after 120 min. Apart from strong ionic interactions in amorphous salts, strong CEL-
460 polymer interactions in both the ASSDs prevented the aggregation of CEL particles from
461 the supersaturated solution. Under non-sink conditions, the ASSD prepared with
462 HPMCAS did not generate supersaturation greater than its binary ASD. The CEL release
463 from both the ASSDs was gradual and the ASSD prepared using PVP-VA exhibited better
464 drug release than HPMCAS because of the formation of pores in the PVP-VA matrix
465 during dissolution. The greater the amount of PVP-VA the larger will be the pore size,
466 which would further effect the dissolution[51]. The higher dissolution of ASSD formulations
467 corresponded to their *in vivo* biopharmaceutical performance.

468 *In vivo pharmacokinetic studies.* The *in vivo* performance of the amorphous formulations
469 was assessed by pharmacokinetic studies. Crystalline CEL showed a maximum plasma
470 concentration (C_{max}) of 21 ng/mL at 1 h whereas CEL-PVP-VA and CEL-HPMCAS
471 binary ASDs showed C_{max} of 56 ng/mL (at 2 h) and 52 ng/mL (at 1 h), respectively. The
472 CEL-K-PVP-VA and CEL-Na-PVP-VA ASSDs exhibited higher C_{max} values of 167
473 ng/mL and 116 ng/mL, respectively, at 12 h whereas the CEL-Na-HPMCAS ASSD
474 attained a C_{max} of 84 ng/mL at 1 h, which further reduced with time. Also, the CEL-K-
475 HPMCAS ASSD acquired a lower C_{max} of 60 ng/mL, even at 12 h (Fig. 6C). Thus, CEL-
476 K-PVP-VA and CEL-Na-PVP-VA ASSDs had approximately 8.0 and 5.6-fold higher
477 C_{max}, respectively, than crystalline CEL. Moreover, the extent of enhancement in C_{max} and
478 other pharmacokinetic parameters was much greater for the ASSD than the binary ASD,
479 see Table 3. Both the ASSD formulations of CEL with PVP-VA possessed a higher
480 plasma concentration of CEL for 12 h due to maintenance of supersaturation for a
481 prolonged period (synergistic effect of amorphization and salt form), enhanced solubility
482 and dissolution, and increased intermolecular drug-polymer interactions in the ionic state
483 than in the neutral state, thereby inhibiting drug-drug aggregation as revealed from the
484 experimental and *in silico* computational interaction studies. This may be ascribed to
485 generation of CEL-rich nano-droplets or a colloidal system in equilibrium with the
486 molecularly dissolved CEL[52]. Also, the PVP-VA matrix allowed higher CEL loading, and
487 enabled carrier-controlled release for continuous dissolution of CEL through gel-like layer
488 of PVP-VA, and absorption into the blood stream gradually over a longer time period[51].
489 However, the binary ASD showed lower supersaturation potential then the ASSD due to
490 weak intermolecular interactions between CEL and PVP-VA, resulting in a lower C_{max} (56
491 ng/mL). Additionally, the formulations with HPMCAS did not prove better than PVP-VA,
492 indicating the lower supersaturation potential of HPMCAS that is evident from its lower
493 solubility at lower pH (10% below pH 4 and 50% at pH 5). Notably, the solid dispersion
494 of paclitaxel (PTX) with HPMCAS-MF failed to improve the oral bioavailability of PTX
495 in Sprague Dawley (SD) rats despite maintenance of *in vitro* supersaturation[53].

496 **Evaluation of formulation stability**

497 The physical stability of the ASSDs was evaluated at ambient conditions and compared to
498 that of the corresponding binary ASDs. All the ASSD formulations were found to be
499 stable for more than 11 months (352 days) at the ambient temperature and relative
500 humidity present in the lab. Even after 11 months storage, DSC thermograms of ASSD
501 formulations prepared with Na^+ or K^+ counterions showed no recrystallization and no
502 melting endotherm (see Fig. S10). The DSC thermograms correlated well with the optical
503 and polarised light microscopy data which showed no birefringence in polarised mode
504 (see Fig. S11). The results support the amorphous nature of the formulations and the
505 absence of recrystallization, indicating the prolonged physical stability of ASSD
506 formulations. ASDs, on the other hand, showed a melting endotherm in DSC thermograms
507 after 11 months, suggesting recrystallization occurred and indicating poor physical
508 stability (see Fig. S10). Consistently, in optical and polarized light microscopy images,
509 birefringence was observed in the polarized mode, confirming the presence of crystallinity
510 in the samples and the loss of the amorphous nature (see Fig. S11). Hydrogen bonds in the
511 ASDs were not able to prevent crystallization over longer time periods whereas the
512 stronger ionic interactions in the ASSDs could. Thus, the ASSD formulation enhanced the
513 physical stability of the amorphous form over long times in comparison to conventional
514 ASDs.

515 **Scanning electron microscopy (SEM) for structural characterization of formulations**
516
517 The surface morphology was observed for the ASD and ASSD formulations using SEM
518 (see Fig. S12). The CEL-Na-PVP-VA ASSD revealed a mixture of spherically shaped
519 smaller and larger particles, with curved surfaces inside the core. This may be due to the
520 drying of particles from the surface during spray drying process. On the other hand, the
521 CEL-PVP-VA ASD showed spherical particles with a collapsed structure. For the CEL-
522 Na-HPMCAS ASSD, spherical particles were observed with irregular surfaces, whereas
523 the CEL-HPMCAS ASD showed irregular shaped particles which were collapsed and
524 highly engraved. The ASSDs prepared with the K^+ counterion showed spherical particles
525 with collapsed structures on the surface. The morphology of the CEL-K-HPMCAS ASSD
526 was more irregular due to highly collapsed surface which may be due to evaporation of
527 solvent from the surface as well as from the core of the particles during spray drying. In
528 the ASSD formulations, the higher solute concentration in the droplets might have led to
529 the faster drying of particles, and the vapor pressure due to the solvent produced smoother
530 particles. On the other hand, a relatively slow rate of solvent evaporation, because of the
531 lower solute content in the drying droplets, might have resulted in shrinkage of the
532 particles, leading to the generation of rough surfaces in the ASDs.
533
534
535 **DISCUSSION**
536
537 The development of next generation ASDs for enhancing the solubility of PWSDs is much
538 needed due to problems of dose dumping and low drug loading capacity, which lead to
539 adverse side-effects, high dosage regimens, and increased overall costs of therapy. Here,
540 we developed advanced ASDs, namely amorphous salt solid dispersions (ASSDs), of
541 CEL, a widely used anti-inflammatory drug that is a PWSD. These ASSDs alleviate many
542 of the problems of conventional ASDs. Although it is established that polymers and salts
543 can play an important role in solubilizing and stabilizing PWSDs, the detailed mechanisms
544 governing the properties of ASDs are poorly understood. The effect of polymers on
545 intermolecular drug-drug interactions in both ionic and neutral states of the drug in
546 aqueous phase are largely unexplored and the basis for the selection of an optimal salt-
547 polymer combination for a particular drug is unclear. Therefore, we here performed *in*
548 *silico* MD simulations of drug-salt-polymer systems in an aqueous environment and
549 compared the results to experimental measurements of *in vitro* properties and the *in vivo*
550 fate of the drug. Atomic detail MD simulations of such systems have only recently
551 become feasible due to the large size and chemical heterogeneity of excipient polymers,
552 making it necessary to simulate systems with large numbers of atoms for long times to
553 obtain sufficient sampling. Thus, the MD simulations were carried out to explore the
554 effects of polymers and ions on drug-drug interactions and drug aggregation, but drug
555 crystallization processes were not simulated as they take place on much longer timescales
556 than the nano-microsecond durations of the MD simulations.
557
558 We focused on ASDs containing CEL, and one of two established polymer excipients -
559 PVP-VA or HPMCAS - with or without Na^+ or K^+ salts. While classical empirical models
560 showed adequate miscibility of CEL and both polymers, they were unable to correctly
561 identify the best drug-salt-polymer combination. In contrast, more stable drug-polymer
562 intermolecular interaction energies computed from the atomically detailed MD
563 simulations were found to correlate with prolonged stability of supersaturated amorphous
564 drug-salt-polymer systems. MD simulations revealed that the PVP-VA oligomer formed a

relatively more stable complex with anionic CEL than the neutral form and was a better polymer than HPMCAS for inhibiting precipitation and maintaining supersaturation of CEL for a prolonged time. All simulations of CEL-containing systems were performed in the presence of NaCl and, as no direct effects of the Na^+ ions on the CEL:CEL or CEL:oligomer interactions were observed, similar behaviour would be expected in simulations with K^+ ions. However, some differences in solubility were observed experimentally between ASSDs with the two cations, likely due to the lower polarizability of K^+ compared to Na^+ ions. Thermal stability analysis revealed that the CEL-Na-PVP-VA and CEL-K-PVP-VA formulations exhibited higher glass transition temperature (T_g) values, proffering good physical stability, and various *in vitro* and *in vivo* studies showed correspondingly improved biopharmaceutical performance. This novel technology of amorphous formulation of CEL facilitates *in situ* salt formation within the polymer matrix leading to high drug-loading and prolonged stability, along with ameliorated aqueous solubility, dissolution, and pharmacokinetic profiles, offering the prospect of less frequent administration and lower doses with good patient compliance, and therefore fewer side effects.

It should be noted that the ASSD technology is not suitable for non-ionizable drugs due to their inability to form a salt. In addition, due to the higher hygroscopicity of ASSDs because of salt formation in comparison to ASDs, their applicability could be challenging for more hygroscopic drugs. The ASSD technology remains to be explored for permeability enhancement of biopharmaceutical classification system (BCS) class IV drugs, that have both low permeability and low solubility. Despite such limitations, the ASSD technology has potential for the formulation of ~ 40 % of marketed drugs and ~90 % of molecules in the drug discovery pipeline that are poorly water soluble and have compromised bioavailability.

The PVP-VA ASSDs characterized in this work may, upon further development for industrial production, find direct application for the administration of CEL due to their excellent biopharmaceutical properties and cost-effectiveness compared to formulations currently in use. Indeed, a straightforward scale-up for their production should be feasible. Although we only considered one drug and a limited number of polymer-salt combinations in this study, the combined computational and experimental approach described here is generally applicable to other class of drugs and polymer types and can be used to aid the rational choice of drug-salt-polymer combinations for drug formulation. Moreover, we expect the physical insights gained into the determinants of amorphous formulations to be relevant for the design of drug-salt-polymer combinations for the formulation of the large class of PWSDs. As ASSDs can improve the physical stability, dissolution and bioavailability of pharmaceutical drugs, we expect them to be particularly valuable in reducing the dosage and side-effects of drugs that show adverse events on prolonged use against a wide range of indications, including anticancer agents, immunosuppressants, antibiotics and antidiabetics. Finally, the ASSD technology could pave the way for biowaivers due to the immediate release of more than 85 % of the drug from the ASSD formulations within 15 to 30 minutes of dissolution, as required by USFDA guidelines for immediate-release drug products[54]; this would provide the dual benefit of cost and time by circumventing the need for *in vivo* bioequivalence studies.

MATERIALS AND METHODS

Experimental design. The experimental and computational characterizations of the systems studied were performed in parallel and the results compared. The systems were chosen to allow systematic comparison of the effects of two polymers – HPMCAS and PVP-VA in the presence or absence of Na^+ or K^+ salts on the physicochemical and biopharmaceutical properties of CEL when formulated as amorphous (salt) solid dispersions. The experiments were designed with the aim of identifying the determinants of system behaviour at supersaturation in aqueous phase and of drug bioavailability.

Materials. CEL form III was provided as a gift sample by Jubilant Generics Ltd. (Noida, Uttar Pradesh, India). PVP-VA, manufactured by BASF (Germany) and HPMCAS-MF grade, manufactured by Shin Estu (Japan) was generously provided by Signet Chemical Corporation Pvt. Ltd. (Mumbai, India). NaOH and KOH were procured from Himedia Laboratories Pvt. Ltd. (Mumbai, India). All other chemicals used in the experiments were of analytical grade and used as such.

Determination of drug-polymer miscibility. Estimation of δ by the Fedors and HVK methods is the conventional approach to calculate drug-polymer miscibility in order to prepare thermodynamically stable amorphous solid based formulations[55,56]. The drug and polymer are found to be miscible if both have similar δ values with the difference in the solubility parameters (Δδ) being less than 7 $MPa^{1/2}$. The Hildebrand solubility parameter for the CEL-PVP-VA and CEL-HPMCAS systems was calculated using Fedors method from the cohesive energy density (CED) using Equation 1, where E_v is the energy of vaporization, V_m is the molar volume, and CED is the cohesive energy per unit volume[55]. The HVK method considers the dispersive forces, interactions between polar groups, and hydrogen bonding groups as shown in Equation 2, where δ_d, δ_p and, δ_h are the dispersive, polar, and hydrogen bonding solubility parameter components, respectively. These components can be further calculated using Equation 3, where F_{di} (dispersion component), F_{pi} (polar component) and E_{hi} (hydrogen bonding energy) are the group contributions for different components of structural groups and V is the group contribution to molar volume[55]. Further, the lattice-based F-H interaction parameter, χ was estimated using the δ value describing the change in Gibbs free energy before and after mixing of drug and polymer as shown in Equation 4, where χ refers to the square of the difference in δ value of the drug and the polymer, calculated from group contribution methods at 25 °C, R is the gas constant, T is the absolute temperature, and V_{site} is the volume per lattice site[55].

$$\boldsymbol{\delta = (CED)^{0.5} = \left(\frac{\Delta E_v}{V_m}\right)^{0.5}} \quad \textbf{(1)}$$

$$\boldsymbol{\delta_{Coh}^2 = \delta_d^2 + \delta_p^2 + \delta_h^2} \quad \textbf{(2)}$$

$$\boldsymbol{\delta_d = \frac{\sum F_{di}}{V},\ \delta_p = \frac{\sqrt{\sum F_{pi}^2}}{V},\ \delta_h = \sqrt{\frac{\sum E_{hi}}{V}}} \quad \textbf{(3)}$$

$$\boldsymbol{\chi = \frac{V_{site}(\delta_{drug} - \delta_{polymer})^2}{RT}} \quad \textbf{(4)}$$

Generation of ASSD and binary ASD formulations. The generation of ASSD formulations was previously explained in detail[27]. Briefly, CEL (pKa 11.1) and counterions {K^+ (KOH (pKa 14.7)) or Na^+ (NaOH (pKa 15.7))} were dissolved in

660 methanol in a 1:1 molar ratio to generate Na^+ and K^+ salt solutions. The salt formation is
661 attributable to the pKa difference of more than 2 between CEL and the counterions. The
662 two screened polymers, HPMCAS and PVP-VA, were dissolved separately in another part
663 of methanol. The salt-containing solutions were then separately added to each polymer-
664 containing solution in order to obtain a drug-polymer mass ratio of 6:4, and mixed well by
665 magnetic stirring (see Fig. S1). The resulting solutions were then subjected to drying using
666 a laboratory scale spray dryer (Buchi B-290, mini spray dryer, Buchi Labortechnik AG,
667 Switzerland) set at the parameters of inlet temperature 80 °C, outlet temperature 50 °C,
668 feed pump 12%, aspiration 85%, and air atomization pressure 400 L/h. Binary ASDs were
669 also generated using the same technique by mixing CEL and HPMCAS or PVP-VA in a
670 6:4 ratio in methanol, and then spray drying.
671 **Characterization methods.** The concentration of CEL in samples for solubility
672 and dissolution studies was analysed using a validated high-performance liquid
673 chromatography (HPLC) method employing an HPLC system (Shimadzu Corporation,
674 Kyoto, Japan) with a PDA detector (SPD- M10AVP) and LC solution software as
675 described previously[27]. Optical imaging of powder samples was carried out to determine
676 the morphology using a polarized light microscope (Leica Microsystems GmbH, Wetzlar
677 Germany), and photomicrographs were acquired in both optical and polarised modes at
678 20x magnification using Leica IM 50 (version 1.20) software to determine the crystalline
679 or amorphous nature of samples. The nature of the samples was also confirmed by DSC
680 and PXRD. The sample preparation for DSC studies was done as described previously[27].
681 A Q2000 DSC (TA Instruments, New Castle, Delaware, USA) with an attached
682 refrigerated cooling system and operating with Universal Analysis software version 4.5A
683 (TA Instruments, New Castle, Delaware, USA) was used. Dry nitrogen at a 50 mL/min
684 flow rate was used to purge the sample cell. The instrument was calibrated for temperature
685 and heat flow using a high purity indium standard. Accurately weighed samples (4-5 mg)
686 in aluminium pans were analysed by heating at a rate of 20 °C/min from 25 °C to 200 °C.
687 The T_g and endothermic transitions were reported as the midpoint temperatures. Powder
688 X-ray diffractograms for crystalline CEL and the generated ASSDs and ASDs were
689 acquired at ambient conditions employing a Rigaku Ultima IV fully automatic high
690 resolution X-ray diffractometer system (Rigaku Corporation, Tokyo, Japan) equipped with
691 an X-ray radiation source Cu Kα tube at 1.54 Å wavelength that was operated at 40
692 kV/40mA, with a divergent slit of 0.5°, a divergent height limit slit of 10 mm, a scattering
693 slit (SS) of 8.0 mm, and a receiving slit (RS) of 13 mm. All the samples were scanned
694 continuously at a step size of 0.02° and scan rate of 15 seconds, over the range from 3° to
695 50° at an angle 2θ and data was analysed using OriginPro 9.1 software (OriginLab Corp.,
696 Northampton, USA).
697 The molecular level drug-polymer interactions in the prepared formulations were
698 investigated using the following high-end analytical techniques. FTIR spectra were
699 recorded on an FTIR multiscope spectrophotometer (PerkinElmer, Buckinghamshire, UK)
700 equipped with Spectrum v3.02 software by a conventional KBr pellet method. The Micro-
701 Raman Jobin Yvon HORIBA LABRAM HR-800 visible system (Kyoto, Japan) equipped
702 with a 473 nm diode laser source, 1800 lines/mm grating, and an Olympus BX41
703 microscope was used to perform Micro-Raman spectroscopy. Raman spectra were
704 recorded in back-scattering mode at room temperature with a pinhole size of 50 µm, slit
705 width of 100 µm and exposure time of 10 seconds and analysed using OriginPro 9.1.
706 Proton NMR was carried out for all the samples dissolved in deuterated DMSO-d6 using a
707 Bruker 500 UltraShield NMR spectrometer (Billerica, Massachusetts, USA) functioning at
708 500 MHz and observation of the chemical shift values was done using MNova14.3.1
709 (MestreLab Research, Santiago de Compostela, Spain).

710 Supersaturation and precipitation studies were conducted with a UV
711 spectrophotometer (SpectraMax® M2 series) and software SoftMax Pro 6.2.1 (Molecular
712 Devices, USA). The sample was immersed in 25 mL of water (aqueous media) at 37 °C
713 for 4 hours by cuvette method. Plain crystalline CEL previously dissolved in methanol at 5
714 mg/mL concentration and drug-polymer samples (ASSD and binary ASD) containing the
715 equivalent of 5 mg CEL were added to the aqueous media while stirring with a magnetic
716 stirrer and the samples were analysed at the absorbing wavelength of 252 nm at reading
717 intervals of 30 seconds.
718 **Molecular modelling.** The drug-polymer interplay at the molecular level was
719 elucidated by MD simulation to address the role and specificity of the polymer in
720 preventing drug-drug aggregation in supersaturated systems. MD simulations were
721 performed for both neutral and anionic CEL in the presence and absence of polymers,
722 estimating the interaction energies between oligomer:CEL and CEL:CEL complexes. The
723 molecular models of CEL, PVP-VA and HPMCAS were generated for further simulation
724 studies. The coordinates of the neutral form of CEL were retrieved from the crystal
725 structure in the Cambridge Crystallographic Data Centre (CCDC)[46,57]. To model the
726 anionic state of CEL, a hydrogen atom was removed from the sulfonamide group. A PVP-
727 VA 34-mer (Fig. 1B) was generated using the Materials Science Platform Release 2020,
728 (Schrödinger, LLC, New York, NY 2021, USA) by randomly assembling 18 units of
729 vinylpyrrolidone (VP) and 16 units vinyl acetate (VA). The mass-ratio of these two units
730 (VP:VA) in the model polymer was roughly equivalent to 6:4. A model of a hypromellose
731 (HPMC) 20-mer was kindly provided by Prof. Ronald G. Larson, (Department of
732 Chemical Engineering, University of Michigan, Ann Arbor, Michigan 48109-2136, USA).
733 We removed 5 monomeric units and then converted the side chain hydroxyl (-OH) group
734 of HPMC to acetyl, deprotonated succinoyl, methoxy and hydroxypropoxy groups using
735 Maestro (Schrödinger version 2020) to build a HPMCAS 15-mer. We chose the side-chain
736 substitutions corresponding to the composition of M-grade HPMCAS[58] (Fig. 1C).
737 Consequently, the modelled 15-mer-M-grade HPMCAS polymer contained 45
738 substituents having 5 different functional groups in the following proportions (given as %
739 of the number of functional groups and by weight (%wt)): methoxy (64.4%; 25%wt),
740 hydroxypropoxy (8.9%; 8.3%wt), acetyl (11.1%; 8.3%wt), succinate (8.9%; 13%wt) and
741 hydroxyl groups or no substitution (6.7%; 1.3%wt).

742 **Molecular parameterization.** GAFF[59] parameters were assigned to CEL and the
743 polymers. Partial atomic charges for both CEL and the polymers were generated by the
744 RESP[60] method as implemented in Antechamber in the AMBER version 14 software
745 package[61] with the Gaussian 09[62] software with B3LYP-6-31G*/HF-6-31G* level of
746 theory[63-66] being used for the electrostatic potential (ESP) calculations. For the polymers,
747 geometry optimization followed by ESP calculations for the entire oligomers would be too
748 computationally demanding. Therefore, RESP charges were computed for each
749 monomeric unit separately. For this purpose, the monomeric units were built with
750 blocking groups to account for the adjacent units. For PVP-VA, six non-terminal and two
751 terminal (see Fig. S9) monomeric units were modelled. Likewise, for HPMCAS (Fig. 1C),
752 13 non-terminal monomeric units were generated by adding an isopropyl group to each of
753 the two terminal oxygen atoms, and 2 terminal monomeric units were generated by adding
754 an isopropyl group to the first and last terminal oxygen atom of HPMCAS. To maintain
755 charge neutrality of the oligomers, the residual charge (-1.646e for the PVP-VA 34-mer
756 and +1.926e for the HPMCAS 15-mer) after assigning the RESP charges to the
757 monomers, which is due to the capping of the terminal atoms of the monomers, was
758 distributed equally onto all the atoms in the oligomers. The TIP3P[67] model was used for
759 water molecules.

760 **Refinement of polymer models by MD simulation.** To structurally refine the
761 polymer models, all-atom MD simulations in explicit solvent were carried out for the two
762 representative model structures of PVP-VA and HPMCAS. The polymers were immersed
763 in cubic periodic boxes using the Gromacs[68] insert-molecules command and then TIP3P
764 water molecules were added to the system using the tleap module of AMBER. To avoid
765 periodicity artifacts, the box dimensions were greater than the lengths of oligomers (see
766 Table 1). 4 excess Na+ ions were added to neutralize the HPMCAS oligomer. The MD
767 simulation protocol is given below. The last snapshot from each trajectory was extracted
768 and used as the starting structure for drug-polymer simulations. The simulation lengths,
769 box sizes and the numbers of water, ions are listed in Table 2 (systems a and b).

770 **Simulation of CEL aggregation.** To simulate a supersaturated solution of CEL,
771 we generated periodic boxes with the same number of CEL molecules as used for the
772 drug-oligomer systems described below. 11 and 13 CEL molecules, which were modelled
773 in either neutral or anionic forms, were inserted randomly in cubic periodic boxes of water
774 molecules with a box-length of 106 and 112 Å, respectively, using the Gromacs insert-
775 molecules and gmx solvate commands. Na^+ ions were added to neutralize each system and
776 thus the Na^+:CEL mass-ratio for each simulated system with anionic CEL molecules was
777 0.0603:1, while in the experiments, the NaOH:CEL ratio was 0.105:1. Note that the
778 hydroxide anions (OH^-) are expected to extract the proton from the CEL sulfonamide
779 nitrogen at higher pH values, and therefore the simulated systems did not contain
780 hydroxide ions. In addition, further Na^+ and Cl^- ions were added to all the simulation
781 boxes to generate ~0.01M ionic solutions (see Table 2). Then, the hydrogen atoms of the
782 water molecules were removed and the residue name of water changed to WAT and the
783 entire system was input to tleap to set it up for simulation with AMBER. All-atom explicit
784 solvent energy minimization and MD simulations were carried out for all the systems and
785 the aggregation of CEL was monitored. The simulation lengths, box sizes and the numbers
786 of water, ions are given in Table 2 (systems c-f).

787 **Simulation of CEL-polymer systems.** For each of the CEL-oligomer
788 combinations listed in Table 2 (systems g-j), one oligomer and several CEL molecules
789 were placed randomly in a periodic simulation box using the Gromacs insert-molecules
790 command, followed by packing of the boxes with water molecules and ions using the gmx
791 solvate command. A typical dose of CEL is 100 to 200 mg given BD (twice a day) with or
792 without food (https://go.drugbank.com/drugs/DB00482). The water content in an empty
793 stomach is typically 35 ml[69]. Thus, the stomach is a supersaturated system with CEL
794 concentration of 1731.6 times higher than its experimental equilibrium solubility (3.46
795 mg/L)[27]. The molecular weights of the model PVP-VA 34-mer, M-grade HPMCAS 15-
796 mer, and CEL are 3375.5, 3691.5, and 381.3 Da, respectively. Hence, to mimic the
797 situation in the experiments, the CEL:oligomer mass ratio in our model systems was
798 chosen to be 1:0.68 for PVP-VA and 1:0.88 for HPMCAS. Thus, one PVP-VA 34-mer
799 and 13 CEL molecules were inserted in a cubic box of length 112 Å, and one HPMCAS
800 15-mer and 11 CEL molecules were inserted in a cubic box of length 106 Å. Afterwards,
801 Na^+ and Cl^- ions were added (see Table 2), and the systems were re-solvated with the tleap
802 module of AMBER as aforementioned and then, all atom explicit solvent energy
803 minimization followed by MD simulations and post-facto trajectory analysis were
804 performed.

805 **MD simulation protocols.** All the systems were energy minimized using the
806 AMBER v14 and v20 software[60]. Energy minimization was carried out by restraining non-
807 hydrogen solute atoms with a force constant that gradually decreased from 1000 to 0
808 kcal/mol·$Å^2$. During energy minimization, the maximum number of cycles was set to

14000 steps: 1400 steps steepest descent followed by 12600 steps conjugate gradient. Minimization was stopped when the root mean square energy gradient for the input coordinates was less than 0.00001 kcal/mol/Å.

MD equilibration and production runs were performed using the AMBER v20 software starting with the energy minimized coordinates. Each system was first equilibrated at constant volume and temperature (NVT) (with the AMBER parameter NTB=1) for a total of 16 ns with a time step of 2 fs at 300 K using the Particle Mesh Ewald (PME) method for long range electrostatic interactions with a non-bonded cut-off of 10 Å. The SHAKE algorithm[70] was imposed to constrain all the bonds to hydrogen atoms. The Langevin dynamics method with a damping coefficient of 5/ps was used for temperature control. The first 6 ns of equilibration was carried out by gradually reducing the restraint force constant from 100 to 10 kcal/mol·$Å^2$ on all non-hydrogen solute atoms. Then the remaining 10 ns of equilibration were run without harmonic restraints. The subsequent production runs were performed for times depending on the convergence of structural parameters, with a time step of 2 fs and a temperature of 300 K in an NPT ensemble (constant number of particles, pressure and temperature were maintained). All simulations were run in duplicate with the same initial coordinates but with different velocities assigned. Coordinates were written at 2.5 ps intervals throughout the simulations.

Analysis of MD trajectories. Analysis of the trajectories was performed using AMBER CPPTRAJ[71]. The RMSD was computed for the frames collected along the simulations and hydrogen bond and radial distribution function (RDF) analysis was carried out for the fully equilibrated part of the trajectories. MM/GBSA solvation and interaction free energy[72,73] calculations were carried out for frames extracted at 100 ps intervals from the same equilibrated parts of the trajectories (Table 1). To compute the drug-drug aggregation energy using the MM/GBSA method, for each extracted frame, we considered each CEL molecule, one at a time, in the drug aggregate (i^{th} celecoxib where "i" is an integer number) and then computed the interaction energy between this molecule and the rest of the aggregate. The CEL-CEL interaction energy was the value computed by averaging over all the CEL molecules in the simulated system and over all the extracted frames. The CEL-oligomer interaction energy was estimated similarly by, for each frame, computing the interaction energy of each CEL molecule with the rest of the complex, i.e.; oligomer and all the remaining CEL molecules, and then subtracting the CEL:CEL aggregation energy from the energy of the CEL:oligomer-CEL system to give the CEL:oligomer interaction energy. The final CEL-oligomer interaction energy was then obtained as the average interaction energy over all frames and overall CEL molecules for each replica trajectory. The average and standard deviation of the MM/GBSA interaction free energy over the replicas was then computed.

Xmgrace (plasma-gate.weizmann.ac.il/Grace/) was used for plotting. Molecular visualization was performed with PyMOL (Version 2.0, Schrödinger, LLC, New York, USA) or VMD[74].

Apparent solubility and *in vitro* dissolution studies. Apparent solubility studies were carried out in distilled water in triplicate, maintained at 37 ± 0.5 °C using a shaking water bath operated at 100 rpm. An excess amount of solid (20 mg) was added to 15 mL of water and aliquots of 1 mL were withdrawn at predetermined time points up to 6 h. All the samples were immediately centrifuged at 15,000 rpm for 10 min and the supernatant was collected for analysis. *In vitro* dissolution studies were conducted in triplicate for the prepared ASSD formulations, the binary ASDs, the physical mixture (PM) [of CEL, polymers and NaOH/KOH mixed geometrically in a mortar using a spatula], and crystalline CEL using a tablet dissolution apparatus (USP 37, type II) (TDT-08L,

Electrolab, Mumbai, India) with an autosampler. The dissolution medium used was 0.04 M tribasic sodium phosphate at pH 12 (under sink conditions) [recommended by the Office of Generic Drugs (OGD), USFDA] and at pH 11 (under non-sink conditions) without surfactant (SLS). A dose equivalent to 100 mg of CEL was added to 1000 ml of dissolution medium maintained at 37 ± 0.5 °C and at 50 rpm. A sample volume of 5 mL was withdrawn at predetermined time intervals up to 120 min, filtered through a 0.22 µm syringe filter (Nylon, MDi membrane filters, Advanced Microdevices Pvt. Ltd., (Ambala Cantt, India)), and the same volume of dissolution medium was supplied instantly after sample withdrawal to maintain sink conditions, whereas no replacement of media was done for non-sink conditions. The CEL concentration in the collected samples after suitable dilution for both solubility and dissolution studies was determined by the validated HPLC method detailed in Tables S3 and S4 and Fig. S13.

***In vivo* pharmacokinetic studies.** *In vivo* pharmacokinetic studies were conducted in SD rats (female, weight: 200 ± 30 g). The CPCSEA (Committee for the Purpose of Control and Supervision of Experiments on Animals) guidelines were followed for performing animal studies. The protocol for animal studies (IAEC/19/51-R) was sanctioned by the Institutional Animal Ethics Committee, NIPER, Mohali, India. All the animals were exposed to 12 h light-dark cycles at 25 °C and 60 % RH for one week and were fasted for 12 h with free access to water before the start of experiments. 7 groups, each consisting of 5 animals, were used for testing six formulations viz. CEL-Na-PVP-VA and CEL-K-PVP-VA; ASSD, CEL-Na-HPMCAS and CEL-K-HPMCAS; ASSD, binary CEL-PVP-VA and CEL-HPMCAS; ASD, and pure crystalline CEL. All formulations were administered orally via oral gavage at a dose of 10 mg equivalent of CEL/kg of rat body mass. Blood samples of approximately 150-200 µL were collected from the tail vein at predetermined time points up to 48 h. Plasma was separated from the blood samples by centrifugation at 10,000 rpm for 10 min at 4 °C and stored at −40 °C before analysis in HPLC. The analysis was done with the bioanalytical method developed using indomethacin as an internal standard. The pharmacokinetic parameters, C_{max}, T_{max}, mean residence time (MRT) and $t_{1/2}$, were derived from the mean plasma concentration−time profiles using the Thermo Kinetica software (V5.0, Thermo Fischer Scientific, USA).

Stability studies. ASSDs and binary ASDs were evaluated for physical stability at ambient conditions in closed containers. Samples were evaluated by polarised light microscopy for detection of birefringence, and by DSC for detecting melting endotherm, indicating the presence of crystallinity in amorphous formulations.

Scanning electron microscopy (SEM). SEM studies were performed for generated ASSDs and ASDs. The surface morphology of powder samples was viewed under a scanning electron microscope (S-3400, Hitachi Ltd., Tokyo, Japan) operated at an excitation voltage of 25 kV. The powder samples were mounted onto a steel stage using double-sided adhesive tape and sputter-coated with gold using ion sputter (E-1010, Hitachi Ltd., Tokyo, Japan), before analysis.

Statistical analysis. The statistical data analysis was done by one-way analysis of variance (ANOVA) using GraphPad Prism 9 software, version 9.1.0 (221) (GraphPad Software, LLC. San Diego, USA). The results were considered statistically significant when $p < 0.05$.

DATA AND MATERIALS AVAILABILITY:

All data are available in the main text or the supplementary materials or the repository at zenodo. Materials are available from the authors on reasonable request.

908
909 **REFERENCES**
910
911
912 1. Lakshman, J. P., Cao, Y., Kowalski, J. & Serajuddin, A. T. M. Application of melt
913 extrusion in the development of a physically and chemically stable high-energy
914 amorphous solid dispersion of a poorly water-soluble drug. *Mol. Pharm.* **5**, 994-1002
915 (2008).
916
917 2. Taylor, L. S. and Zhang, G. G. Z. Physical chemistry of supersaturated solutions and
918 implications for oral absorption. *Adv. Drug Del. Rev*. **101,** 122-142 (2016).
919
920 3. Bhujbal, S. V. et al. Pharmaceutical amorphous solid dispersion: a review of
921 manufacturing strategies. *Acta Pharm. Sin. B.* **11**, 2505-2536 (2021).
922
923 4. Wegiel, L. A., Mauer, L. J., Edgar, K. J. & Taylor, L. S. Crystallization of amorphous
924 solid dispersions of resveratrol during preparation and storage-impact of different
925 polymers. *J. Pharm. Sci.* **102,** 171-184 (2013).
926
927 5. Javadzadeh, Y., Dizaj, S. M., Vazifehasl, Z. & Mokhtarpour, M. Recrystallization of
928 drugs-effect on dissolution rate. *Recryst. Mater. Processing* **191**, 211 (2015).
929
930 6. Joshi, P. et al. Explicating the molecular level drug-polymer interactions at the interface of
931 supersaturated solution of the model drug: Albendazole. *Eur. J. Pharm. Sci.* **167**, 106014
932 (2021).
933
934 7. Warren, D. B., Benameur, H., Porter, C. J. H. & Pouton, C. W. Using polymeric
935 precipitation inhibitors to improve the absorption of poorly water-soluble drugs: a
936 mechanistic basis for utility. *J. Drug Target.* **18,** 704-731 (2010).
937
938 8. Metre, S., Mukesh, S., Samal, S. K., Chand, M. & Sangamwar, A. T. Enhanced
939 biopharmaceutical performance of rivaroxaban through polymeric amorphous solid
940 dispersion. *Mol. Pharm.* **15**, 652-668 (2018).
941
942 9. Wilson, V. R. et al. Amorphous solid dispersions of enzalutamide and novel
943 polysaccharide derivatives: investigation of relationships between polymer structure and
944 performance. *Sci. Rep.* **10**, 18535 (2020).
945
946 10. Suys, E. J. A., Chalmers, D. K., Pouton, C. W. & Porter, C. J. H. Polymeric precipitation
947 inhibitors promote fenofibrate supersaturation and enhance drug absorption from a type iv
948 lipid-based formulation. *Mol. Pharm.* **15**, 2355-2371 (2018).
949
950 11. Ilie, A. R. et al. Exploring precipitation inhibitors to improve in vivo absorption of
951 cinnarizine from supersaturated lipid-based drug delivery systems. *Eur. J. Pharm.* Sci.
952 **159,** 105691 (2021).
953
954 12. Koehl, N. J. et al. In silico, in vitro, and in vivo evaluation of precipitation inhibitors in
955 supersaturated lipid-based formulations of venetoclax. *Mol. Pharm.* **18**, 2174-2188 (2021).
956

13. Chen, Z. Q., Liu, Y., Zhao, J. H., Wang, L. & Feng, N. P. Improved oral bioavailability of poorly water-soluble indirubin by a supersaturatable self-microemulsifying drug delivery system. *Int. J. Nanomed.* **7**, 1115-1125 (2012).

14. Feng, D. et al. Polymer-surfactant system based amorphous solid dispersion: precipitation inhibition and bioavailability enhancement of itraconazole. *Pharmaceutics* **10**, 53 (2018).

15. Schittny, A., Philipp-Bauer, S., Detampel, P., Huwyler, J. & Puchkov, M. Mechanistic insights into effect of surfactants on oral bioavailability of amorphous solid dispersions. *J. Control. Release* **320**, 214-225 (2020).

16. Clemett, D. & Goa, K. L. Celecoxib: a review of its use in osteoarthritis, rheumatoid arthritis and acute pain. *Drugs* **59**, 957-80 (2000).

17. Dougados, M. et al. Efficacy of celecoxib, a cyclooxygenase 2-specific inhibitor, in the treatment of ankylosing spondylitis: a six-week controlled study with comparison against placebo and against a conventional nonsteroidal antiinflammatory drug. *Arthritis Rheum*. **44**, 180-5 (2001).

18. Ward, M. M. Nonsteroidal anti-inflammatory drugs: disease modifiers in ankylosing spondylitis? *Nat. Clin. Pract. Rheumatol.* **1**, 18-19 (2005).

19. *Global Celecoxib Market Growth 2021-2026*. *Market Research Insights,* 130 https://www.marketreportsworld.com/enquiry/request-sample/19852767 (2021).

20. Nguyen, H. V., Park, C., Oh, E. & Lee, B. J. Improving the dissolution rate of a poorly water-soluble drug via adsorption onto pharmaceutical diluents. *J. Drug Deliv. Sci. Technol.* **35**, 146-154 (2016).

21. Cserháti, T., Forgács, E. & Oros, G. Biological activity and environmental impact of anionic surfactants. *Environ. Int.* **28**, 337-48 (2002).

22. Kosswig, K. Surfactants. *Ullmann's Encycl. Ind. Chem*. **35**, 431-505 (2012).

23. Kwon, H. J. et al. Development and evaluation of poorly water-soluble celecoxib as solid dispersions containing nonionic surfactants using fluidized-bed granulation. *Pharmaceutics* **11**, 136 (2019).

24. Paulson, S. K. et al. Pharmacokinetics of celecoxib after oral administration in dogs and humans: effect of food and site of absorption. *J. Pharmacol. Exp. Ther.* **297,** 638-45 (2001).

25. Bijlsma, J. W. J. Celecoxib-fewer gastrointestinal adverse events in patients with osteoarthritis. *Nat. Clin. Pract. Rheumatol.* **2**, 414-415 (2006).

26. Aronson, J. K. COX-2 inhibitors (coxibs) *Meyler's Side Effects of Drugs*, 738-762 (2016).

27. Mukesh, S. et al. Amorphous salts solid dispersions of celecoxib: enhanced biopharmaceutical performance and physical stability. *Mol. Pharm.* **18**, 2334-2348 (2021).

1007 28. Panakanti, R. & Narang, A. S. Impact of excipient interactions on drug bioavailability
1008 from solid dosage forms. *Pharm. Res.* **29**, 2639-59 (2012).
1009
1010 29. Ishizuka, Y. et al. Effect of drug-polymer interactions through hypromellose acetate
1011 succinate substituents on the physical stability on solid dispersions studied by fourier-
1012 transform infrared and solid-state nuclear magnetic resonance. *Mol. Pharm.* **16**, 2785-
1013 2794 (2019).
1014
1015 30. Yu, D. et al. Role of polymers in the physical and chemical stability of amorphous solid
1016 dispersion: A case study of carbamazepine. *Eur. J. Pharm. Sci.* **169**, 106086 (2022).
1017
1018 31. Patel, D. D. & Anderson, B. D. Effect of precipitation inhibitors on indomethacin
1019 supersaturation maintenance: mechanisms and modeling. *Mol. Pharm.* **11**, 1489-1499
1020 (2014).
1021
1022 32. Singh, R. et al. Elucidating the molecular mechanism of drug-polymer interplay in a
1023 polymeric supersaturated system of rifaximin. *Mol. Pharm.* **18,** 1604-1621 (2021).
1024
1025 33. Marsac, P. J., Li, T. & Taylor, L. S. Estimation of drug–polymer miscibility and solubility
1026 in amorphous solid dispersions using experimentally determined interaction parameters.
1027 *Pharm. Res.* **26**, 139 (2009).
1028
1029 34. Meng, F., Dave, V. & Chauhan, H. Qualitative and quantitative methods to determine
1030 miscibility in amorphous drug–polymer systems. *Eur. J. Pharm. Sci.* **77,** 106-111 (2015).
1031
1032 35. Phadke, C., Sharma, J., Sharma, K. & Bansal, A. K. Effect of variability of physical
1033 properties of povidone K30 on crystallization and drug-polymer miscibility of celecoxib-
1034 povidone K30 amorphous solid dispersions. *Mol. Pharm.* **16**, 4139-4148 (2019).
1035
1036 36. Li, C., Wang, J. X., Le, Y. & Chen, J. F. Studies of bicalutamide-excipients interaction by
1037 combination of molecular docking and molecular dynamics simulation. *Mol. Pharm.* **10**,
1038 2362-9 (2013).
1039
1040 37. Gupta, J., Nunes, C., Vyas, S. & Jonnalagadda, S. Prediction of solubility parameters and
1041 miscibility of pharmaceutical compounds by molecular dynamics simulations. *J. Phys.*
1042 *Chem. B* **115**, 2014-2023 (2011).
1043
1044 38. Huang, W., Dalal, I. S. & Larson, R. G. Analysis of solvation and gelation behavior of
1045 methylcellulose using atomistic molecular dynamics simulations. *J. Phys. Chem. B* **118**,
1046 13992-14008 (2014).
1047
1048 39. Li, Q. et al. Investigating molecular interactions of high-loaded glipizide-HPMCAS
1049 microparticles by integrated experimental and modeling techniques. *Eur. J. Pharm. Sci.*
1050 **131**, 127-135 (2019).
1051
1052 40. Huang, W., Mandal, T. & Larson, R. G. Computational modeling of hydroxypropyl-
1053 methylcellulose acetate succinate (HPMCAS) and phenytoin interactions: a systematic
1054 coarse-graining approach. *Mol. Pharm.* **14**, 733-745 (2017).
1055

41. Huang, W., Mandal, T. & Larson, R. G. Multiscale computational modeling of the nanostructure of solid dispersions of hydroxypropyl methylcellulose acetate succinate (HPMCAS) and phenytoin. *Mol. Pharm.* **14**, 3422-3435 (2017).

42. Dong, J., Gao, H. & Ouyang, D. PharmSD: A novel AI-based computational platform for solid dispersion formulation design. *Int. J. Pharm.* **604**, 120705 (2021).

43. Gao, H., Wang, W., Dong, J., Ye, Z. & Ouyang, D. An integrated computational methodology with data-driven machine learning, molecular modeling and PBPK modeling to accelerate solid dispersion formulation design. *Eur. J. Pharm. Biopharm.* **158**, 336-346 (2021).

44. Murphy, D. B., Spring, K. R., Fellers, T. J. & Davidson, M. W. Principles of Birefringence [MicroscopyU]. https://www.microscopyu.com/techniques/polarized-light/principles-of-birefringence.

45. Gupta, P., Thilagavathi, R., Chakraborti, A. K. & Bansal, A. K. Differential molecular interactions between the crystalline and the amorphous phases of celecoxib. *J. Pharm. Pharmacol.* **57**, 1271-8 (2005).

46. Remenar, J. F. et al. Celecoxib sodium salt: engineering crystal forms for performance. *Cryst. Eng. Comm.* **13**, 1081-1089 (2011).

47. Mähler, J. & Persson, I. A study of the hydration of the alkali metal ions in aqueous solution. *Inorg. Chem.* **51**, 425-438 (2012).

48. Andrews, G. P. et al. Physicochemical characterization and drug-release properties of celecoxib hot-melt extruded glass solutions. *J. Pharm. Pharmacol.* **62**, 1580-90 (2010).

49. Friesen, D. T. et al. Hydroxypropyl methylcellulose acetate succinate-based spray-dried dispersions: an overview. *Mol. Pharm.* **5**, 1003-1019 (2008).

50. Serajuddin, A. T. M. Salt formation to improve drug solubility. *Adv. Drug Deliv. Rev.* **59,** 603-616 (2007).

51. Školáková, T. et al. Investigation of dissolution mechanism and release kinetics of poorly water-soluble tadalafil from amorphous solid dispersions prepared by various methods. *Pharmaceutics* **11**, 383 (2019).

52. Schittny, A., Huwyler, J. & Puchkov, M. Mechanisms of increased bioavailability through amorphous solid dispersions: a review. *Drug Deliv*. **27**, 110-127 (2020).

53. Miao, L. et al. Effect of supersaturation on the oral bioavailability of paclitaxel/polymer amorphous solid dispersion. *Drug Deliv. Transl. Res.* **9**, 344-356 (2019).

54. Reddy, N. H. S., Patnala, S., Lobenberg, R. & Kanfer, I. *In vitro* dissolution of generic immediate-release solid oral dosage forms containing BCS class I drugs: comparative assessment of metronidazole, zidovudine, and amoxicillin versus relevant comparator pharmaceutical products in South Africa and India. *AAPS PharmSciTech*. **15**, 1076-86 (2014).

55. Van Krevelen, D. W. & Nijenhuis, K. T. Properties of polymers: their correlation with chemical structure; their numerical estimation and prediction from additive group contributions. 4th Edition, *Elsevier B.V.* (2009).

56. Medarević, D., Djuris, J., Barmpalexis, P., Kachrimanis, K. & Ibric, S. Analytical and computational methods for the estimation of drug-polymer solubility and miscibility in solid dispersions development. *Pharmaceutics* **11**, 372 (2019).

57. Groom, C. R., Bruno, I. J., Lightfoot, M. P. & Ward, S. C. The cambridge structural database. *Acta. Crystallogr. B. Struct. Sci. Cryst. Eng. Mater.* **72**, 171-179 (2016).

58. *AquaSolve*™ Hypromellose Acetate Succinate (HPMCAS) https://www.ashland.com/file_source/Ashland/Industries/Pharmaceutical/Links/PC-12624.6_AquaSolve_HPMCAS_Physical_Chemical_Properties.pdf, Ashland, Covington, KY, USA (2016).

59. Wang, J., Wolf, R. M., Caldwell, J. W., Kollman, P. A. & Case, D. A. Development and testing of a general amber force field. *J. Comput. Chem.* **25**, 1157-74 (2004).

60. Bayly, C. I., Cieplak, P., Cornell, W. & Kollman, P. A. A well-behaved electrostatic potential based method using charge restraints for deriving atomic charges: the RESP model. *J. Phys. Chem.* **97**, 10269-10280 (1993).

61. Salomon-Ferrer, R., Case, D. A. & Walker, R. C. An overview of the amber biomolecular simulation package. *Wiley Interdiscip. Rev. Comput. Mol. Sci.* **3**, 198-210 (2013).

62. Frisch, M. J. et al. Gaussian 09, Revision E. 01, Gaussian. Inc., Wallingford CT, USA (2013).

63. Hehre, W. J., Ditchfield, R. & Pople, J. A. Self—consistent molecular orbital methods. xii. further extensions of gaussian—type basis sets for use in molecular orbital studies of organic molecules. *J. Chem. Phys.* **56,** 2257-2261 (1972).

64. Vosko, S. H., Wilk, L. & Nusair, M. Accurate spin-dependent electron liquid correlation energies for local spin density calculations: a critical analysis. *Can. J. Phys.* **58**, 1200-1211 (1980).

65. Lee, C., Yang, W. & Parr, R. G. Development of the Colle-Salvetti correlation-energy formula into a functional of the electron density. *Phys. Rev. B Condens. Matter.* **37**, 785-789 (1988).

66. Raghavachari, K. Perspective on "density functional thermochemistry. III. the role of exact exchange", in theoretical chemistry accounts: new century issue. *Springer Berlin Heidelberg: Berlin, Heidelberg.* 361-363 (2001).

67. Jorgensen, W. L., Chandrasekhar, J., Madura, J. D., Impey, R. W. & Klein, M. L. Comparison of simple potential functions for simulating liquid water. *J. Chem. Phys.* **79,** 926-935 (1983).

68. Lindahl, E., Abraham, M. J., Hess, B. & Spoel, D. V. GROMACS development team, GROMACS 2021.2 Manual. https://manual.gromacs.org/2021.2/index.html, (2021).

69. Mudie, D. M. et al. Quantification of gastrointestinal liquid volumes and distribution following a 240 ml dose of water in the fasted state. *Mol. Pharm.* **11,** 3039-3047 (2014).

70. Kräutler, V., van Gunsteren, W. F. & Hünenberger, P. H. A fast SHAKE algorithm to solve distance constraint equations for small molecules in molecular dynamics simulations. *J. Comput. Chem.* **22,** (2001).

71. Roe, D. R. & Cheatham, T. E. PTRAJ and CPPTRAJ: software for processing and analysis of molecular dynamics trajectory data. *J. Chem. Theory Comput.* **9,** 3084-3095 (2013).

72. Kollman, P. A. et al. Calculating structures and free energies of complex molecules: combining molecular mechanics and continuum models. *Acc. Chem. Res.* **33**, 889-897 (2000).

73. Lyne, P. D., Lamb, M. L. & Saeh, J. C. Accurate prediction of the relative potencies of members of a series of kinase inhibitors using molecular docking and MM-GBSA scoring. *J. Med. Chem*. **49**, 4805-8 (2006).

74. Humphrey, W., Dalke, A. & Schulten, K. VMD: visual molecular dynamics. *J. Mol. Graph.* **14**, 33-8, 27-8 (1996).

Acknowledgments

We thank Prajwal P. Nandekar for his contributions in the initial phases of this study, Giulia Paiardi for helpful discussions and assistance with data archiving, and Stefan Richter for technical support for the computational work.

Funding:
German Federal Ministry for Education and Research (BMBF) 01DQ19004 (RCW)
Klaus Tschira Foundation (GM, NS, CD, RCW)
Baden-Württemberg bwHPC for computing resources (RCW)
German Research Foundation (DFG) grant INST 35/1134-1 FUGG for computing resources (RCW)
Department of Biotechnology, New Delhi, BT/IN/BMBF-BioHR/34/ATS/2018-19 (ATS).

Author contributions:

Conceptualization: SM, GM, ATS, RCW

Experimental Investigation: SM, PJ

Computational Investigation: GM, NS, CD

Experimental Data Analysis: SM, RS, ATS

Computational Data Analysis: GM, NS, CD, RCW

Visualization: SM, RS, GM

Supervision: ATS, RCW

Writing—original draft, review and editing: RS, SM, GM, ATS, RCW

Competing interests: ATS, SM, GM and RCW are authors on Indian patent application 202011007741A, 16.03.2021 “Novel amorphous pharmaceutical formulations of celecoxib salts in polymeric solid dispersion with improved aqueous solubility and stability”.

Figures and Tables

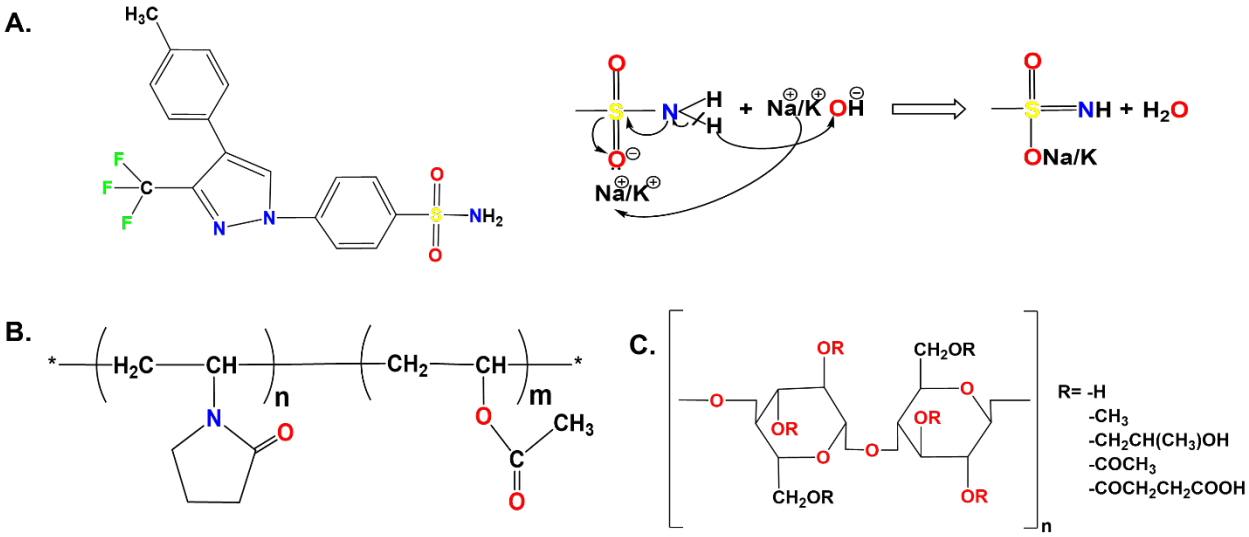

Fig. 1. Chemical structures of CEL and the polymer excipients studied. **(A)** CEL in neutral form with scheme showing the formation of the CEL anionic salt in the presence of NaOH or KOH. **(B)** Poly-(1-vinylpyrrolidone-co-vinyl-acetate) (PVP-VA). (C) Hypromellose acetate succinate (HPMCAS). The M-grade contains acetyl and succinoyl groups at 7-11% and 10-14% weight fractions along with methoxyl and hydroxypropoxyl groups at 21-25% and 5-9%[58].

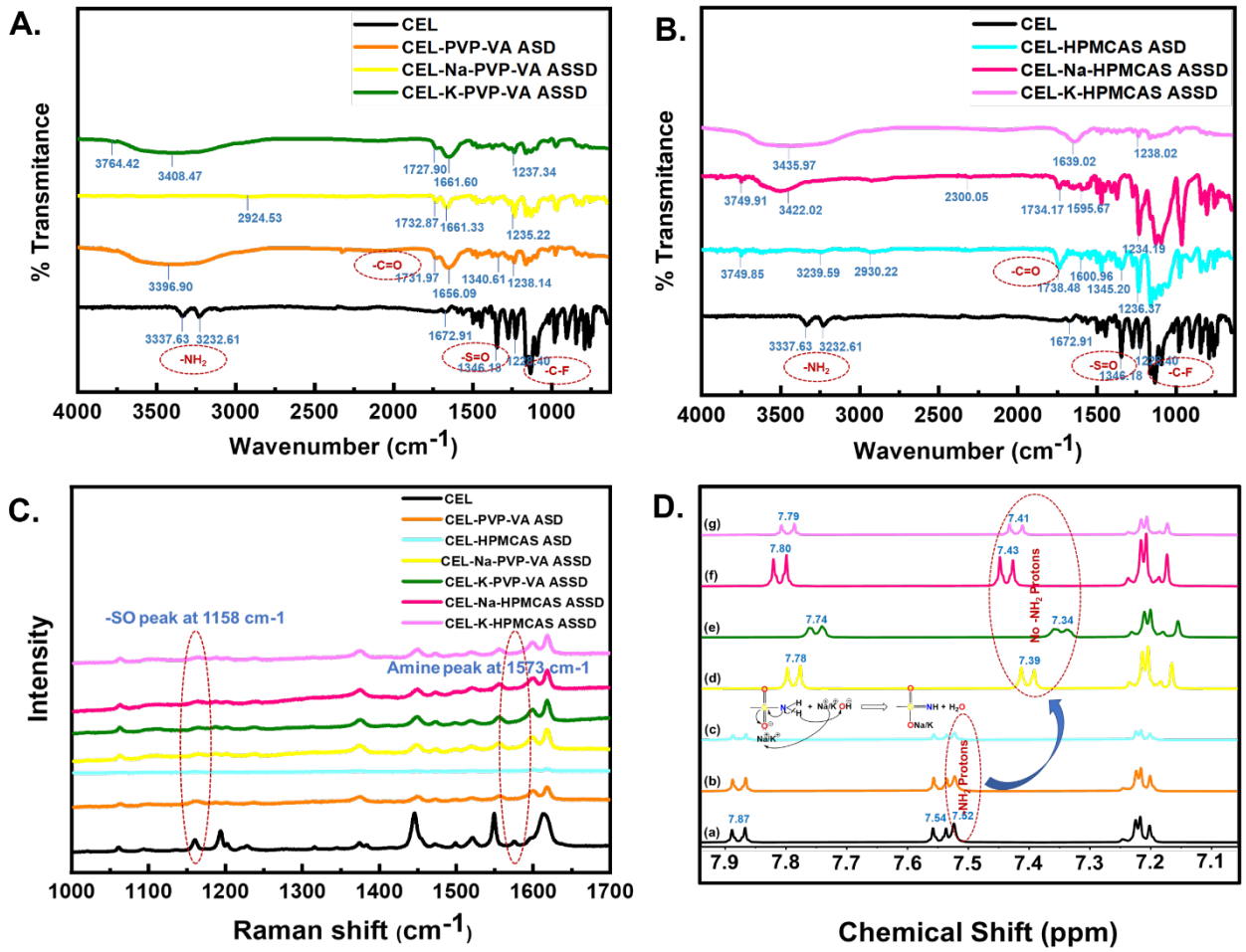

Fig. 2. Spectroscopic techniques reveal intermolecular interactions between CEL and the polymer in amorphous formulations. **(A,B)** FTIR-ATR spectra of CEL and CEL-PVP-VA (A) and CEL-HPMCAS (B) formulations. The spectra show the disappearance of the -S=O peak in ASSDs, indicating the involvement of the -S=O group in salt formation (Figure 1), and broadening of the -NH stretching peak of the $-NH_2$ group in ASDs and ASSDs, revealing the amorphous nature of both formulations. **(C)** Micro-Raman spectra of crystalline CEL and its ASD and ASSD formulations. The spectra for the ASSD formulations show the disappearance of the -S=O peak in the ASSD formations, indicating salt formation, and -NH stretching peak in both ASD and ASSD formulations, revealing the amorphous nature of the formulations. **(D)** NMR spectra between 7.1 and 7.9 ppm of (a) CEL, (b) CEL-PVP-VA ASD, (c) CEL-HPMCAS ASD, (d) CEL-Na-PVP-VA ASSD, (e) CEL-K-PVP-VA ASSD, (f) CEL-Na-HPMCAS ASSD and (g) CEL-K-HPMCAS ASSD. The complete spectral region is shown in Fig. S5. The spectra show the upfield shift in the aromatic protons of CEL at 7.87 and 7.54 ppm and the disappearance of the $-NH_2$ proton peak at 7.52 ppm in the ASSD formulations, indicating salt formation.

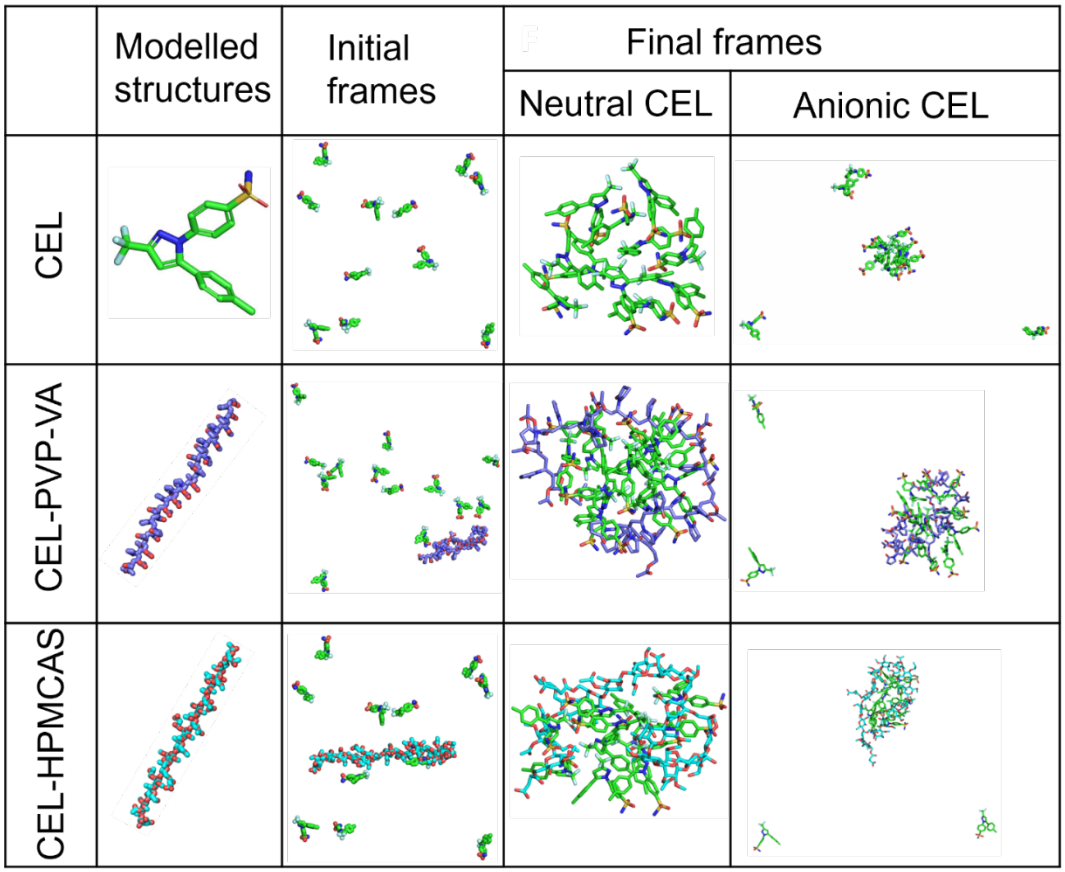

Fig. 3. Modelled structures of the molecules simulated and snapshots of initial and final frames of the simulated systems of CEL alone and CEL with either PVP-VA or HPMCAS. Initially, the CEL molecules were placed in random positions and orientations in a periodic box of solvent without or with an oligomer. The final frames for the simulation times given in Table 2 are shown for simulation replica-1 for systems with neutral or anionic forms of CEL. For the neutral form of CEL, aggregation of the CEL molecules alone or with the oligomer is observed during all the simulations. For the anionic form of CEL, a lower aggregation propensity was observed with some CEL molecules remaining free during the simulations (the final snapshot after simulation for 916 ns for anionic CEL without oligomer is shown for system e but in system f, which also lacked oligomer (Table 2), no aggregation of anionic CEL molecules was observed in a simulation of 1042 ns duration).

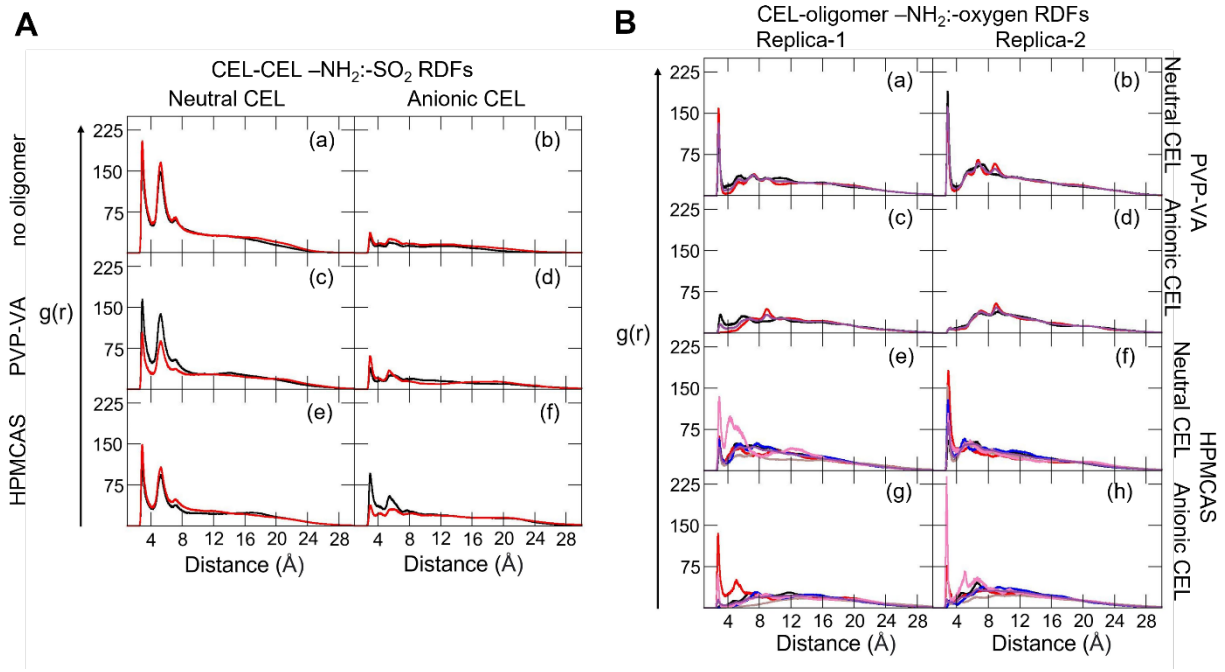

Fig. 4. Radial distribution functions (RDFs) computed from all-atom explicit solvent MD simulations showing CEL-CEL and CEL-oligomer intermolecular interactions. (A). Intermolecular CEL:CEL RDFs between the sulfonamide -NH_2 group of one CEL molecule and the SO_2 group of another (replica-1: black, replica-2: red) for the neutral (left) and anionic (right) forms of CEL without polymer (a,b), with PVP-VA (c,d), and with HPMCAS (e,f). The RDFs show reduced neutral CEL-CEL interactions in the presence of polymer and tend to zero with increasing distance because the molecules aggregate. **(B).** Intermolecular CEL:oligomer RDFs computed from the replica-1 (left) and replica-2 (right) MD simulations. RDFs are shown for: the sulfonamide -NH_2 group of the neutral (a,b) and anionic (c,d) forms of 13 CEL molecules and the carbonyl oxygen atoms of vinyl acetate (black) and vinylpyrrolidone (red) moieties and all oxygen atoms (purple) of the PVP-VA oligomer; sulfonamide -NH_2 group of neutral (e,f) and anionic (g,h) forms of 11 CEL molecules and oxygen atoms of methoxy (black), hydroxypropoxy (red), succinoyl (brown), acetyl (blue), hydroxy (pink) and all oxygen atoms (purple) of the HPMCAS oligomer.

1289

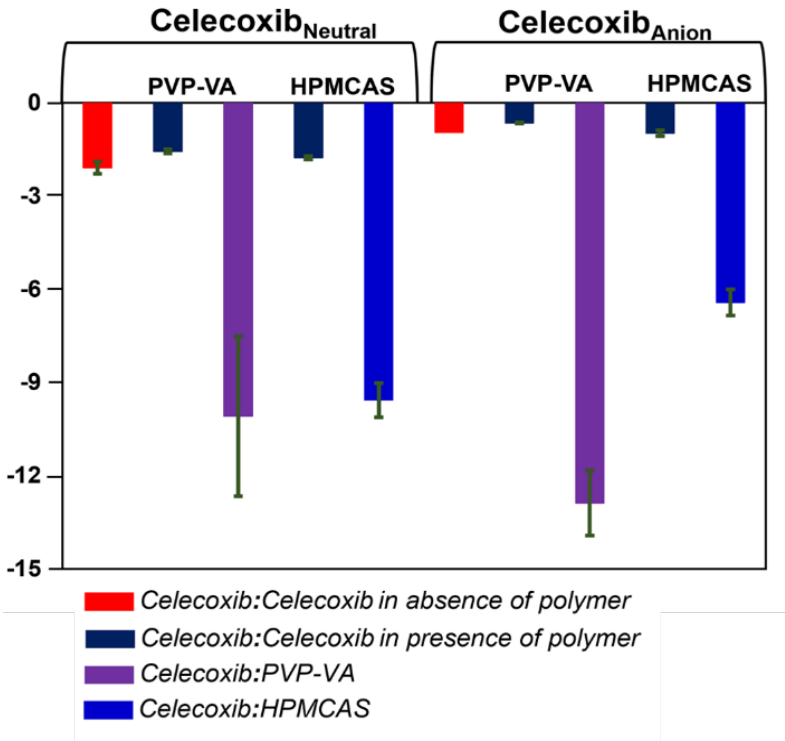

1290 **Fig. 5. Computed interaction energies for the drug and drug-polymer systems**
1291 **indicate suitable polymer excipients.** Computed MM/GBSA energies (kcal/mol)
1292 for the CEL:CEL (red, deep blue), CEL:PVP-VA (purple) and CEL:HPMCAS
1293 (blue) interactions show more energetically favorable interactions of PVP-VA with
1294 CEL than HPMCAS, particularly for the anionic form of CEL, with
1295 correspondingly energetically weaker CEL:CEL interactions. These trends are
1296 consistent with the better excipient properties of PVP-VA for the CEL ASSD. The
1297 averages and standard deviations of the energies computed from a set of snapshots
1298 from the two replica simulations for each system are shown. Computed values are
1299 given in Table S1 and their decomposition is given in Table S2.

1300
1301

1302

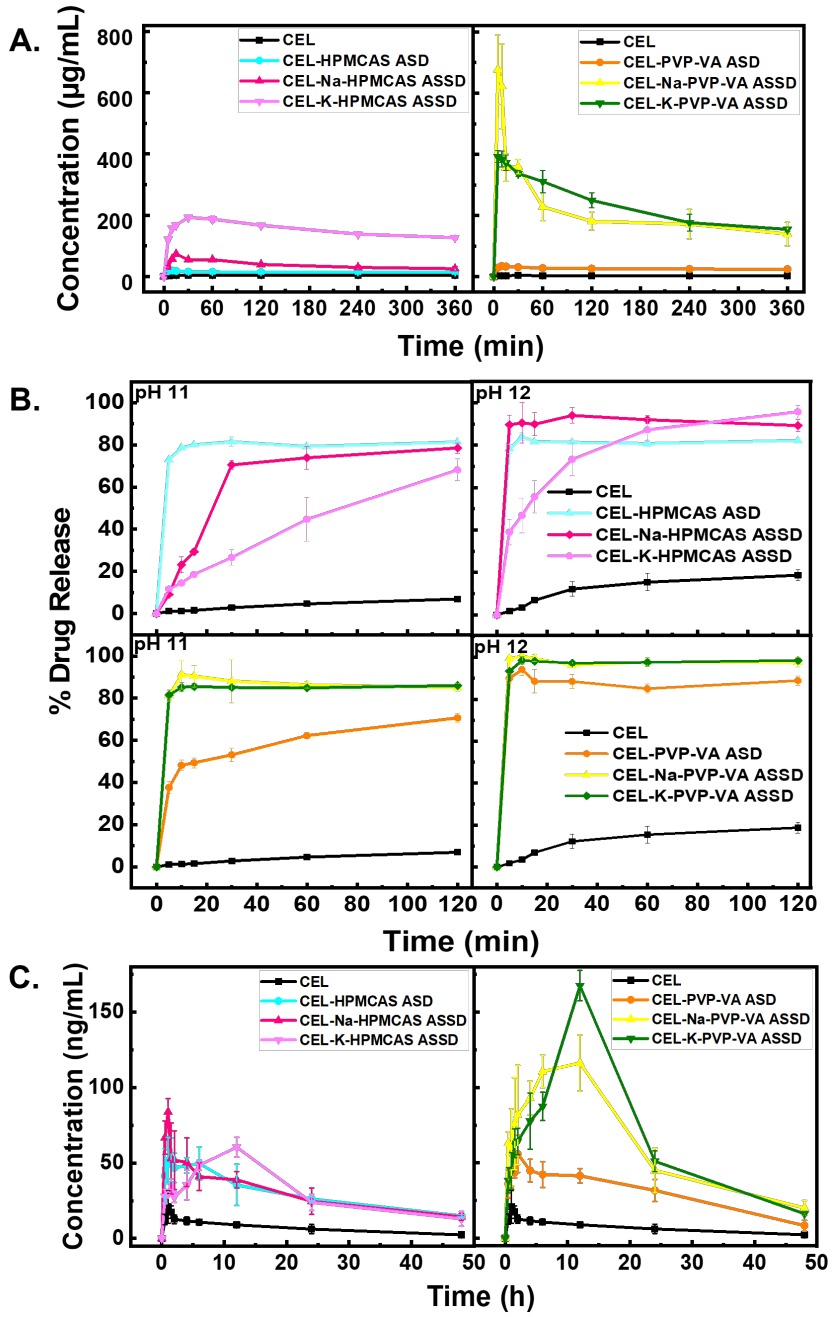

1303 **Fig. 6. Biopharmaceutical properties of crystalline CEL and its amorphous**
1304 **formulations, showing the best performance for the CEL-PVP-VA salts. (A)**
1305 Apparent solubility in aqueous medium (water) for 6 h. **(B)** Dissolution profile
1306 under sink and non-sink conditions in pH 11 and 12 buffer media, respectively, for
1307 2 h as per OGD recommendation for dissolution performance. Measurements for
1308 (A) and (B) were made in triplicate. **(C)** Plasma concentration vs time profile from
1309 pharmacokinetic studies performed for 48 h in SD female rats (n=5; data provided
1310 in accompanying Excel file).

1311
1312

1313 **Table 1. Solubility parameter values calculated by the Fedors and HVK methods for**
1314 **CEL and the two polymers studied.**

Name of compound	**Fedors method: Hildebrand solubility parameter δ ($MPa^{1/2}$)**	**HVK method: Hansen solubility parameter δ ($MPa^{1/2}$)**	**Mean δ ($MPa^{1/2}$)**	**Δδ ($MPa^{1/2}$) (δ_{drug}-$\delta_{polymer}$)**	**Flory–Huggins (F-H) interaction parameter χ (drug-polymer)**
Celecoxib	23.88	23.82	23.85	--	--
PVP-VA	22.74	22.94	22.84	1.01	0.100
HPMCAS	22.40	24.00	23.20	0.65	0.041

1315
1316

1317 **Table 2. Specifications of the simulated systems to study the aggregation of CEL.** MD
1318 simulations were carried out for polymeric excipients without CEL (a,b), and for
1319 the neutral (c,d,g,i) and anionic (e,f,h,j) forms of CEL in the absence (c-f) and
1320 presence (g-j) of a polymeric excipient. Each drug-polymer system was simulated
1321 in duplicate, generating trajectories referred to as replica-1 and replica-2. For the
1322 systems without polymer, two systems with different initial box sizes were each
1323 simulated once.

1324

System	# of CEL molecules and ionization state	Polymer and its length (Å)	Periodic box size (Å)*	# of water molecules	# of Na^+ ions	# of Cl^- ions	# of replica simul-ations	Simulation length (ns)
a	0	PVP-VA (75.1)	X=154.2; Y= 94.3; Z= 99.9	46569	0	0	1	66
b	0	HPMCAS (79.2)	X =158.2; Y = 127.3; Z = 99.2	58720	4	0	1	66
c	13 neutral	---	112	138672	9	9	1	516
d	11 neutral	---	106	117072	7	7	1	456
e	13 anionic	---	112	138672	22	9	1	916
f	11 anionic	---	106	117066	18	7	1	1042
g	13 neutral	PVP-VA (43.9)	112	46031	9	9	2	356
h	13 anionic	PVP-VA (43.9)	112	46038	22	9	2	356
i	11 neutral	HPMCAS (72.2)	106	38819	11	7	2	376
j	11 anionic	HPMCAS (72.2)	106	38831	22	7	2	376

1325 *The initial box was cubic unless specified by giving the X, Y and Z dimensions.
1326

1327 **Table 3. *In vivo* pharmacokinetic parameters of crystalline CEL, and CEL ASD and ASSD**
1328 **formulations.**

Formulations	C_{max} (ng/mL)	Fold increase	T_{max} (h)	AUC (ng.h/mL)[#]	Fold increase	MRT (h)	$T_{1/2}$ (h)
Crystalline CEL	20.94± 10.85	-	1± 0.28	374.09± 25.98	-	24.09± 2.35	17.5± 1.45
CEL-PVP-VA ASD	55.93± 12.21	2.67	2± 0.5	1632.67± 226.76	1.79	23.44± 3.45	15.14± 3.20
CEL-Na-PVP-VA ASSD	116.23± 18.45*	5.55	12± 0.0	3327.57± 151.68	8.89	22.56± 0.54	14.89± 0.36
CEL-K-PVP-VA ASSD	167.47± 10.02*	7.99	12± 0.0	3519.76± 124.77	9.40	19.26± 0.19	11.12± 0.09
CEL-HPMCAS ASD	51.66± 15.28	2.46	1± 1.73	1615.63± 126.54	4.36	27.18± 3.89	19.11± 3.41
CEL-Na-HPMCAS ASSD	83.89± 8.74	4.00	1± 0.28	1878.63± 101.56	5.02	34.49± 0.98	24.41± 0.85
CEL-K-HPMCAS ASSD	60.49± 6.52	2.88	12± 0.0	1774.5± 192.29	4.74	26.8± 2.86	17.25± 2.36

1329 *$p < 0.05$, statistically significant difference in comparison with crystalline CEL at n=3 (n=
1330 no of animals in each group)

1331 [#]The fold increase represents the fold-enhancement in the C_{max} and AUC of prepared
1332 formulations compared to pure crystalline CEL.

1333
1334